Chapter 4

Mixed Gas Corrosion of Pure Metals

4.1 INTRODUCTION

Atmospheres encountered in practice are very rarely constituted of a single oxidant. Even in the case of air, both oxygen and nitrogen can react with a base metal such as chromium. Examples of more complex gases are frequently encountered.

A common example is provided by combustion gases which invariably contain carbonaceous species, usually water vapour and, commonly, sulphur species deriving from the impurities present in most fossil fuels. Another example is the production of synthesis gas. The two processes used to produce hydrogen on a large scale are steam reforming

$$CH_4 + H_2O = CO + 3H_2 \quad [4.1]$$

and coal gasification

$$C + H_2O = CO + H_2 \quad [4.2]$$

Clearly both processes involve handling gases which, at the necessarily low oxygen potentials, are likely to be carburising as well as oxidising. In general, it is necessary to consider the possibility of more than one oxidant reacting with the metal.

After a brief review of selected experimental findings, the use of phase diagrams and diffusion paths to arrive at an understanding of scale constitutions is examined, and surface processes are analysed. The mechanisms of mass transport are then considered in a discussion of scaling rates. Much of the literature in the area of mixed gas corrosion is of an applied nature, involving complex engineering alloys and simulated, multicomponent process gases. Whilst of obvious practical utility, this literature provides little in the way of fundamental understanding. Fortunately, a substantial number of model studies involving pure metals is also available, particularly for sulphidising-oxidising gases [1–7].

The behaviour of a number of metals in gases containing both oxygen and sulphur was studied rather intensively in the 1970 and 1980s, in the aftermath

High Temperature Oxidation and Corrosion of Metals. http://dx.doi.org/10.1016/B978-0-08-100101-1.00004-2

of sudden oil price increases, when alternative routes to liquid fuels were being sought. There has been renewed interest in the matter, as oil prices rise from time to time, and the combustion of high sulphur content coals for power generation increases. Attention is focused here on the behaviour of chromium, iron and nickel in mixed gases.

4.2 SELECTED EXPERIMENTAL FINDINGS

Key questions in the case of mixed gas corrosion concern whether or not reaction products other than oxide form, and to what extent they are harmful. Iron exposed to SO_2 or SO_2-Ar can form a lamellar mixture of sulphide plus oxide [9,10] or a two-phase mixture overlaid by oxide alone [8,9,11−14], as shown in Fig. 4.1. Layered structures of the sort shown in Fig. 4.2 can be formed on nickel [8,15−17] and sometimes on cobalt [18,19] although results reported for cobalt are not all in agreement.

More complex gas mixtures of $CO/CO_2/SO_2/N_2$ have been used to simulate aspects of combustion gas corrosion and to permit independent control of p_{S_2} and p_{O_2}. The earlier literature concerns reaction in pure SO_2 or in diluted SO_2/Ar mixtures. In these gases the equilibrium

$$SO_2 = \frac{1}{2}S_2 + O_2 \qquad [4.3]$$

requires that $p_{S_2} \approx \frac{1}{2}p_{O_2}$, if SO_3 formation can be neglected. Values of ΔG° [4.3] are given in Table 2.1. In the $CO/CO_2/SO_2/N_2$ mixtures, Eq. [4.3] still holds, but the equilibrium

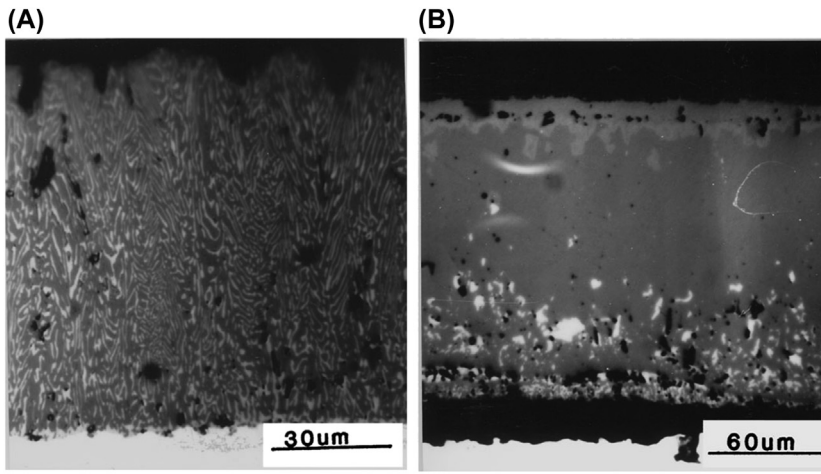

FIGURE 4.1 Oxide-sulphide scales grown on iron in different $SO_2/CO_2/CO$ mixtures at 800°C. Grey phase is oxide, light phase is sulphide.

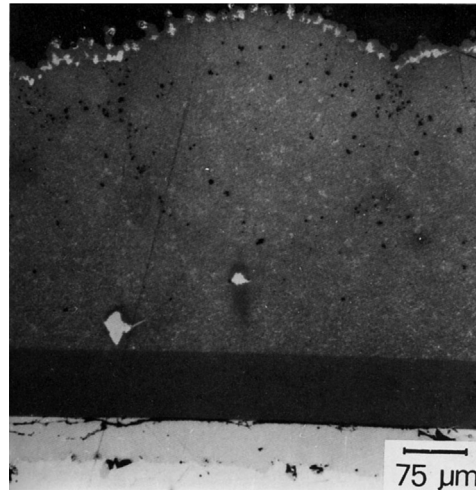

FIGURE 4.2 Layered sulphide-oxide scale grown on nickel in SO_2 at 600°C. *With kind permission from F. Gesmundo, C. DeAsmundis, P. Nanni, Oxid. Met. 20 (1983) 217, Springer Science and Business Media.*

$$CO_2 = CO + \frac{1}{2}O_2 \qquad [4.4]$$

can be used to control p_{O_2}, and the value of p_{S_2} is given by

$$p_{S_2}^{\frac{1}{2}} = K_{4.3} p_{SO_2} / p_{O_2} \qquad [4.5]$$

Additional species such as COS and CS_2 can be important under some conditions. In these cases equilibrium calculations are best carried out using numerical free energy minimisation procedures, such as those in software packages like ThermoCalc or FACTSage.

A practical difficulty arises from the rather slow rates of the homogeneous gas-phase reactions involved, and it is essential that laboratory gas mixtures be brought to equilibrium by passing them through a heated catalyst bed (such as alumina-supported platinum) before contacting the experimental specimen. The effect is illustrated in Fig. 4.3 for manganese exposed at 800°C to a gas mixture of inlet composition 23-CO_2, 45-CO, 22-SO_2, 10-N_2 volume percent. The calculated equilibrium composition contained $p_{S_2} = 8.6 \times 10^{-6}$ atm and $p_{O_2} = 5.7 \times 10^{-16}$ atm. As seen in the figure, the catalysed gas produced a scale of MnO plus MnS, but the noncatalysed gas led to a scale which evolved with time from a two-phase mixture to an almost single-phase MnO.

The formation and behaviour of Cr_2O_3 in mixed gases has been the subject of many research programs because of the protective nature of the Cr_2O_3 scale,

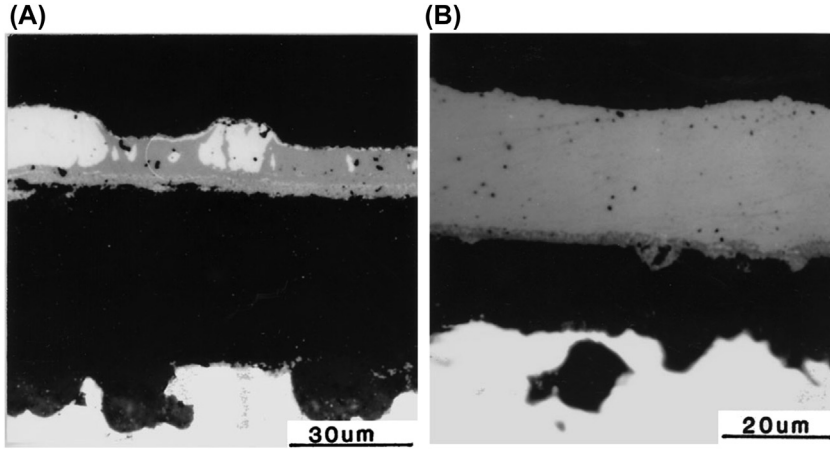

FIGURE 4.3 Scales grown on manganese in $CO_2/CO/SO_2/N_2$ mixture at 800°C (light phase sulphide, grey phase oxide): (A) gas passed over Pt catalyst and (B) gas uncatalysed. At equilibrium, MnS is stable with respect to MnO. *With kind permission from G. McAdam, D.J. Young, Oxid. Met. 37 (1992) 301, Springer Science and Business Media.*

upon which many technologically important alloys depend. In the presence of secondary oxidants, chromia scales have been found to behave in a diversity of ways. For example, a sublayer product of Cr_2N has often been found growing underneath an outer Cr_2O_3 scale on pure chromium after heating in air [21–26]. Preoxidation for 2.5 h in oxygen $\left(p_{O_2} = 40\ \text{kPa}\right)$ was found not to stop the nitridation of chromium during subsequent exposure to nitrogen $\left(p_{N_2} = 40\ \text{kPa}\right)$, indicating that the previously established oxide film does not constitute an effective barrier to nitrogen ingress. Obviously the oxide scale formed under these conditions was not impermeable to gas penetration, and nitrogen from the air had reached the chromium.

When exposed at 900°C to a CO/CO_2 mixture (Table 4.1), chromium is found [27] to develop a two-layered scale (Fig. 4.4A) consisting of a Cr_2O_3 outer layer and an inner layer of Cr_7C_3 containing finely distributed oxide particles. Adding N_2 to $CO\text{-}CO_2$ results in a three-layered scale (Fig. 4.4B). The outer layer is again pure Cr_2O_3. The intermediate layer, now thicker than the chromia, is a mixture of Cr_7C_3, oxide and a small amount of Cr_2N. The innermost layer is pure, compact Cr_2N. In a gas mixture of $H_2/H_2O/N_2$ corresponding to the same equilibrium p_{O_2} value as the $CO/CO_2/N_2$ gas, and a closely similar value of p_{N_2}, chromium grows a single layer of pure Cr_2O_3, and no nitride develops.

Addition of SO_2 to the gas (Table 4.2) leads to sulphide formation and suppresses nitridation [28]. The resulting scale is shown in Fig. 4.4C to be multilayered. The outermost layer is principally Cr_5S_6 with a Cr_2O_3 content varying from 1 wt% at the scale-gas interface to 12 wt% near its inner

TABLE 4.1 Carburising-Oxidising-Nitriding Gas Mixtures Reacted With Chromium [27]

	Starting Gas Composition (Vol%)					Reaction Potentials, 900°C		
Gas No.	CO	CO_2	H_2	H_2O	N_2	$p(O_2)$, atm	$p(N_2)$, atm	a_C
1	96.6	3.40				1×10^{-19}		0.5
2	62.2	2.20			35.6	1×10^{-19}	0.36	0.5
3	49.7	17.6			32.7	1×10^{-17}	0.33	0.04
4	12.4	44.0			43.6	1×10^{-15}	0.44	0.001
5			56.5	2.30	41.2	1×10^{-19}	0.41	

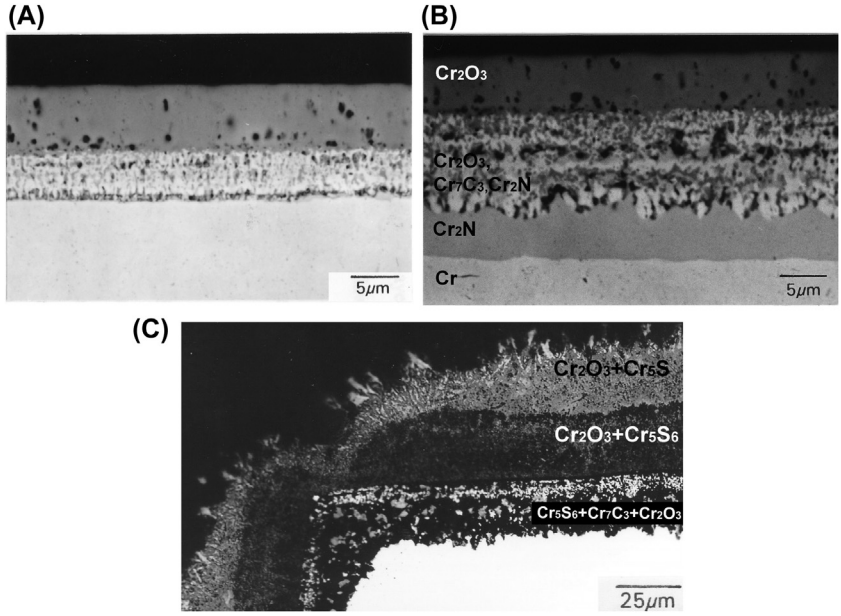

FIGURE 4.4 Scales grown on chromium exposed at 900°C to (A) CO/CO_2, (B) $CO/CO_2/N_2$ *(With kind permission from X.G. Zheng, D.J. Young, Oxid. Met. 42 (1994) 163, Springer Science and Business Media.)*, and (C) $SO_2/CO_2/CO/N_2$ *(Reprinted from X.G. Zheng, D.J. Young, Corros. Sci. 36 (1994) 1999, with permission from Elsevier).*

TABLE 4.2 Sulphur-Bearing Gas Mixtures Reacted With Chromium [28]

	Input Gas Composition (Vol%)				Reaction Potentials (atm) at 900°C			
Gas	CO	CO_2	N_2	SO_2	$p(O_2)$	$p(S_2)$	$p(N_2)$	a_C
A	74.7	2.56	22.7	0.039	1×10^{-19}	3×10^{-7}	0.23	0.6
B	62.2	2.18	35.6	0.010	1×10^{-19}	3×10^{-8}	0.36	0.5
C	74.6	2.63	22.8	0.0039	1×10^{-19}	3×10^{-9}	0.23	0.6

boundary. This two-phase mixture consists of a fibrous structure aligned approximately normally to the metal substrate surface. The underlying scale region is highly porous. Its outer region is largely oxide with a small sulphur content, but its inner region is principally Cr_5S_6 with minor amounts of Cr_2O_3 and Cr_7C_3. The innermost layer is mainly Cr_7C_3 and Cr_2O_3 with very little sulphide.

Lower p_{SO_2} values have less effect [28]. The gas composition represented by point B in Fig. 4.10 produces a thick compact scale of Cr_2O_3 containing about 24 wt% Cr_5S_6 as finely dispersed particles. Gas C (Fig. 4.10) produces an outer, buckled layer of Cr_2O_3 containing 0.5 wt% S. A thin sublayer made up of Cr_7C_3 with oxide dispersions also forms adjacent to the metal.

Rather different observations have been reported for the reaction of chromium in pure SO_2. An early investigation [29] reported the simultaneous growth of CrS and Cr_2O_3, whereas later work [30] using the same gas led to the finding that only oxide formed, containing 1 wt% S. However, scaling rates in SO_2 were found to be two to three orders of magnitude faster than in oxygen at 800−1000°C. The reaction of chromium with $H_2/H_2O/H_2S$ gases at 900°C has also been studied [31]. These gases were such that Cr_2O_3 was stable with respect to sulphides, but two-phase oxide-plus-sulphide scales formed at low H_2O/H_2S ratios. At intermediate ratios, the two-phase product was overgrown by oxide, and at high ratios, only oxide was formed.

Scaling kinetics and rates can vary considerably as the nature of the reaction product changes with gas composition. When iron is reacted with dilute Ar-SO_2 mixtures, an initial period of linear reaction is followed by parabolic kinetics, as shown in Fig. 4.5. Flatley and Birks [9] demonstrated that the linear rate constant was proportional to both p_{SO_2} and the gas flow rate, and they concluded that gas-phase diffusion of SO_2 was rate controlling in this regime. The reaction product was a lamellar oxide-sulphide mixture of the type shown in Fig. 4.1(a). The subsequent parabolic stage of reaction reflected the onset of solid-state diffusion control in the thicker scale. At low p_{SO_2} values, this scale consisted of a coarse FeO + FeS outer layer on top of the

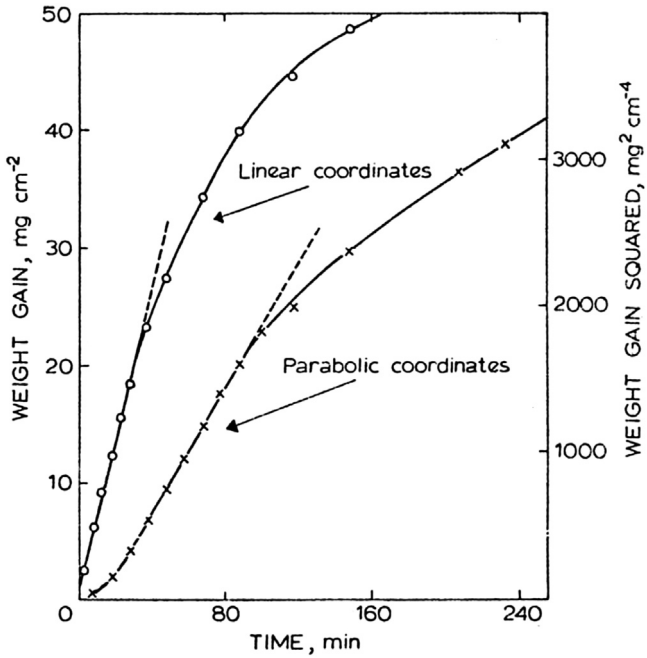

FIGURE 4.5 Initial linear and subsequent parabolic kinetics: Fe reacted with dilute Ar-SO_2 at T = 800°C. *Published with permission from T. Flatley, N. Birks, J.I.S.I. 209 (1971) 523, Taylor and Francis Ltd, http://www.informaworld.com.*

first formed lamellar structure. Reaction rates were reported to be faster than those for the oxidation of iron in pure oxygen. At high p_{SO_2} values, the initially formed FeO + FeS structure was overgrown by pure oxide, and the parabolic rate constant was equal to that for the oxidation of iron in pure O_2 [10]. The same result was found for reaction in $CO/CO_2/SO_2/N_2$ gases [20].

Chromium scaling kinetics in the gas mixtures of Tables 4.1 and 4.2 are shown in Figs. 4.6 and 4.7. The formation of additional carbide and nitride layers augments the rate, and sulphide formation increases the rate by up to an order of magnitude, depending on the sulphur partial pressure.

4.3 PHASE DIAGRAMS AND DIFFUSION PATHS

Thermochemical diagrams of the sort described in Section 2.2 provide a useful basis for analysing and rationalising the morphologies of scales grown in dual oxidant gases. However, as we now discuss, they seldom provide a means of predicting the outcome of a particular reaction.

The essence of this approach is simple: calculate the partial pressures of the two oxidants, locate the coordinates on the thermochemical diagram (Section 2.2) and thereby define the reaction product. Even if this calculation is

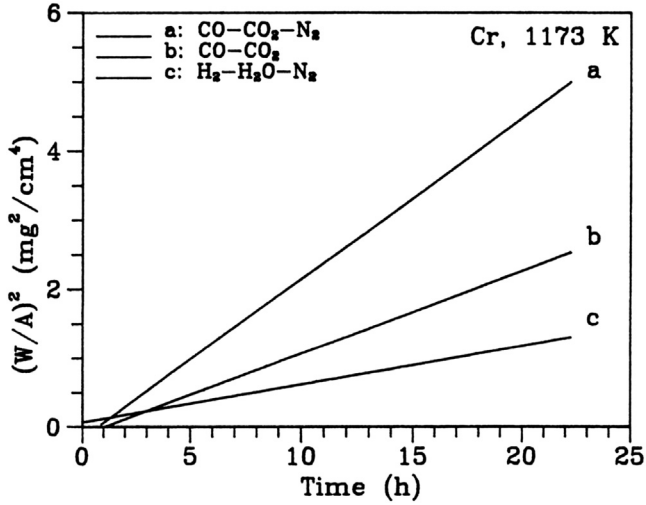

FIGURE 4.6 Chromium scaling kinetics at 900°C in gases of Table 4.1. *With kind permission from X.G. Zheng, D.J. Young, Oxid. Met. 42 (1994) 163, Springer Science and Business Media.*

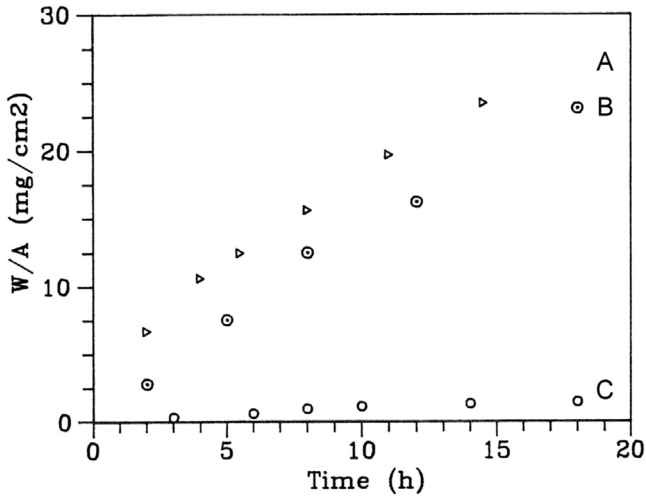

FIGURE 4.7 Chromium scaling kinetics at 900°C in gases of Table 4.2. *Published with permission from X.G. Zheng, D.J. Young, Mater. Sci. Forum 251–254 (1997) 567, Trans Tech Publications Ltd.*

successful, it provides no information as to which compounds will exist within the scale interior, where the oxidant activities are not the same as in the gas. More seriously, the prediction often fails even at the scale-gas interface, where one might hope to predict the equilibrium phase, as is done in the case of a single oxidant (Section 3.2).

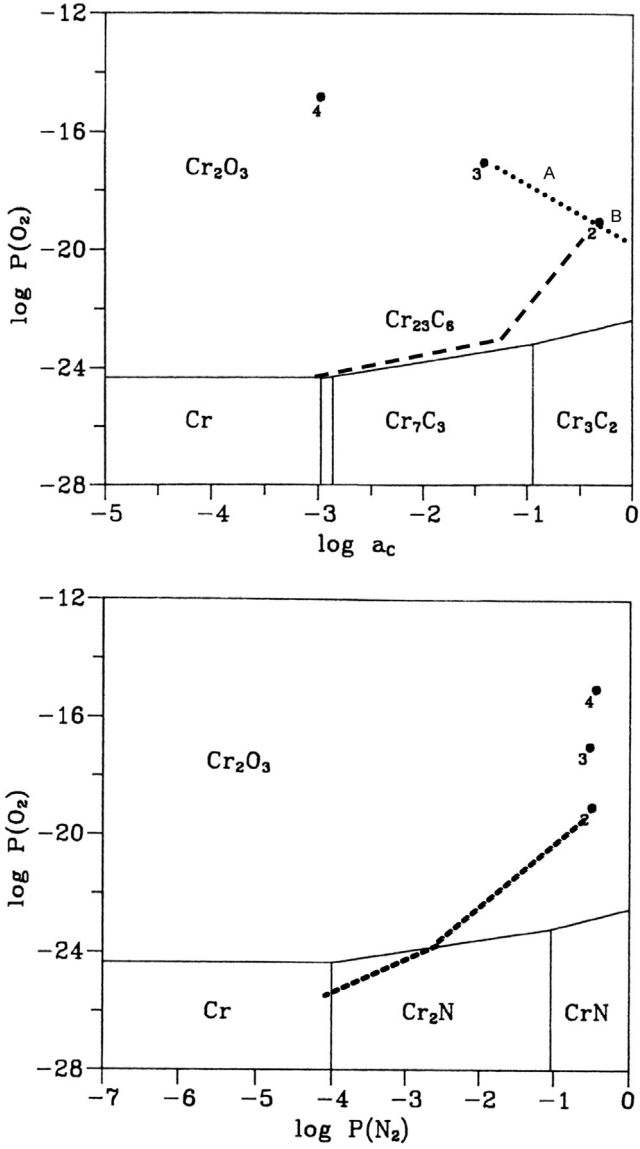

FIGURE 4.8 Thermochemical diagrams for Cr-O-C and Cr-O-N at 900°C. Points correspond to equilibrium for gases in Table 4.1. *Dashed lines* show diffusion paths for oxide-carbide and oxide-nitride scales. The *dotted line* represents equilibrium $C + \frac{1}{2}O_2 = CO$ at fixed p_{CO}.

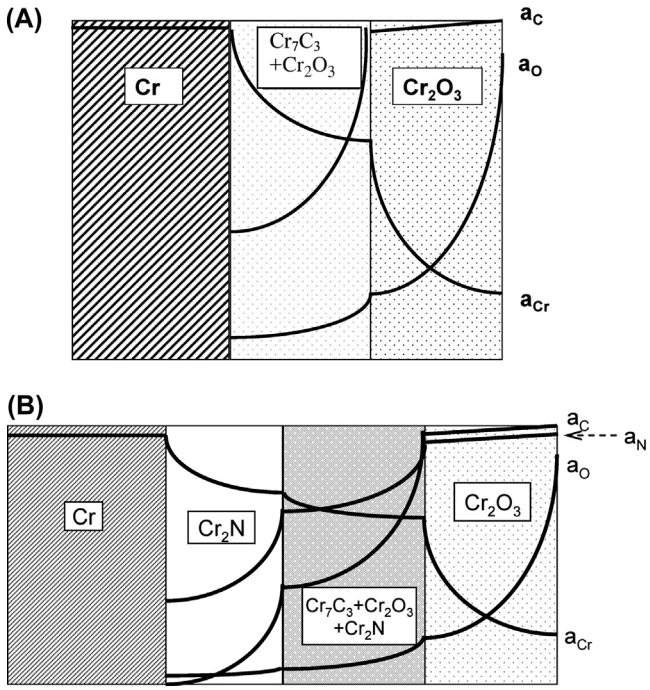

FIGURE 4.9 Schematic activity profiles representing the penetration of (A) carbon and (B) nitrogen and carbon through a Cr_2O_3 layer.

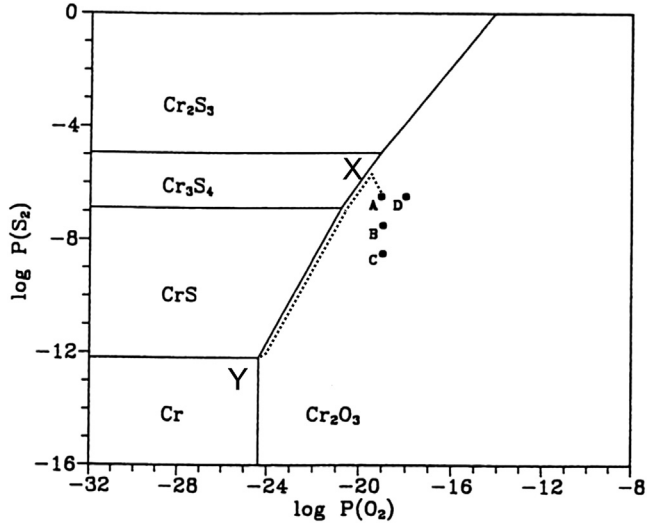

FIGURE 4.10 Thermochemical diagram for Cr-O-S at 900°C. *Dotted line* shows diffusion path for sulphide forming under oxide.

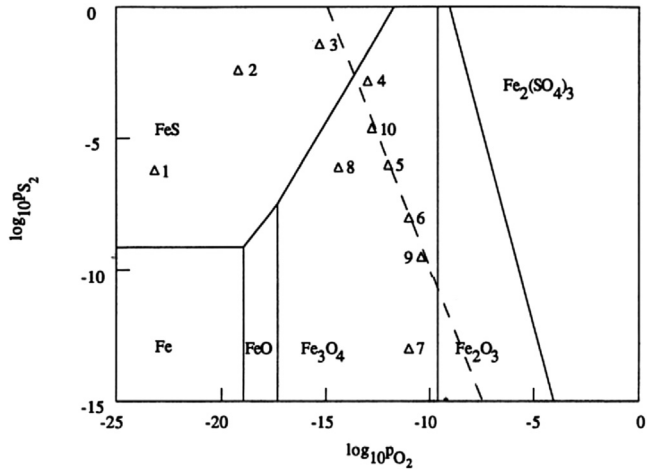

FIGURE 4.11 Thermochemical diagram for Fe-O-S at 800°C. Numbered points represent equilibrium compositions for reaction gases. *Dashed line* represents $p_{SO_2} = 7.9 \times 10^{-2}$ atm. *With kind permission from G. McAdam, D.J. Young, Oxid. Met. 37 (1992) 281, Springer Science and Business Media.*

One reason for such a failure was illustrated in Fig. 4.3. In the absence of a catalyst, the gas phase was far removed from equilibrium and a completely different reaction product resulted. Even in pure SO_2 this can be a problem, because the additional reaction

$$SO_2 + \frac{1}{2}O_2 = SO_3 \qquad [4.6]$$

can, depending on temperature, affect the value of p_{O_2} by orders of magnitude [30]. Unfortunately, much of the early work on reactions with pure or diluted SO_2 failed to employ a catalyst for the SO_3 reaction.

If the scaling reaction is rapid and the reactant species is dilute or at low pressure, then it will be depleted from the gas at the scale surface. In the absence of a catalyst at this surface, the gas composition will be different from that of the bulk gas. Furthermore, the kinetics of the solid-gas reactions can lead to changes in the relative oxidant activities, a point which is discussed in Section 4.2 with reference to oxidation-sulphidation of nickel, cobalt and iron.

We consider first the reactions of chromium with oxygen-carbon and oxygen-nitrogen gases, where scaling rates are slow and the complications described above should be avoided.

4.3.1 Scaling of Chromium in Oxidising-Nitriding and Oxidising-Carburising Gases

The Cr-O-C and Cr-O-N phase diagrams are shown in Fig. 4.8, with the equilibrium oxidant potentials for the gases in Table 4.1 marked. The carbon

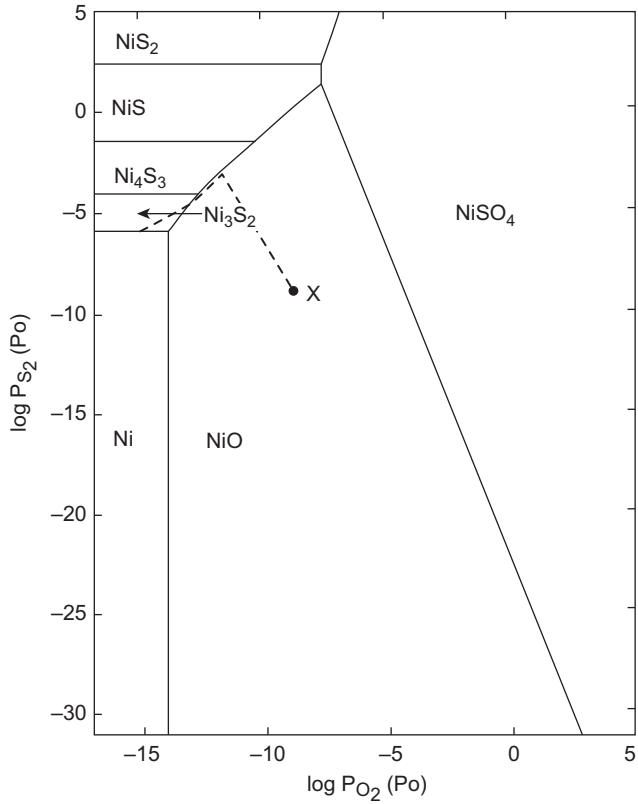

FIGURE 4.12 Thermochemical diagram for Ni-O-S at 600°C. Point X represents equilibrium in pure SO_2 at 1 atm. Diffusion path for oxide + sulphide layer over Ni_3S_2 layer.

activity, a_C, is defined through [2.48], with pure solid graphite as reference state. The oxide is much more stable than both carbide and nitride and is predicted to form in contact with these gases. As seen in Fig. 4.4, the prediction is borne out. Unfortunately, however, the protection expected of a chromia scale is not realised in the CO/CO_2 based gases, or even in air, as carbides and/or nitrides form beneath the oxide. As will be shown subsequently, the inner carbide and nitride layers continue to grow as the chromia layer thickens, showing that carbon and nitrogen are diffusing through the oxide. A schematic diffusion path for the oxide over nitride-layered structure grown in air [21–25] is shown in Fig. 4.8, where the Cr_2O_3/Cr_2N phase boundary is seen to correspond to the interface between the two scale layers.

A diffusion path for the oxide over carbide + oxide layered structure developed in $CO/CO_2/Ar$ is shown in Fig. 4.8. The transit of the path through the inner, two-phase layer is represented by the line along the carbide-oxide phase boundary. Although the activity ratio, a_o/a_C, is defined at this

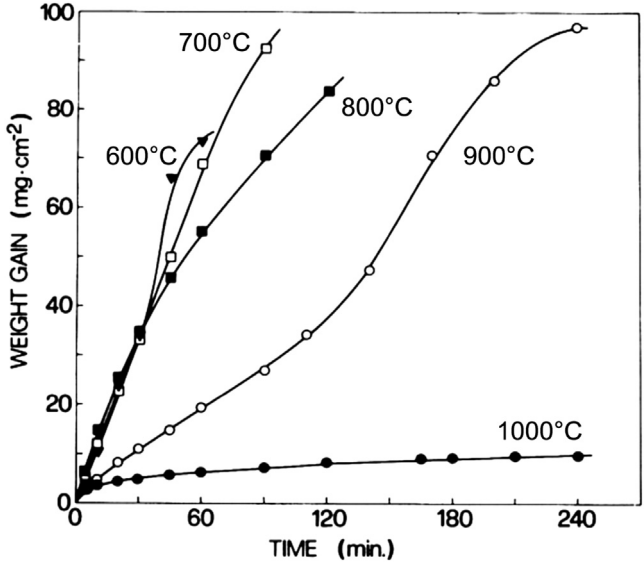

FIGURE 4.13 Scaling kinetics for Ni exposed to SO_2. *With kind permission from F. Gesmundo, C. DeAsmundis, P. Nanni, Oxid. Met. 20 (1983) 217, Springer Science and Business Media.*

boundary (assuming pure, stoichiometric compounds), the individual values are not. Put another way, the three-component system has a degree of freedom in the two-phase region, and the activity gradients necessary for mass transfer and scale growth can and do develop.

The compositions of all the above gases were such that chromium oxide was stable with respect to chromium carbide and nitride. However, the gas-phase carbon and nitrogen activities were high enough to react with chromium in the absence of oxygen. The observed sequence of reaction products in the scales is in accord with thermodynamic prediction. Thus at the scale surface where the chromium activity is lowest, the most stable product, oxide, is formed. At the scale base where the chromium activity is highest and oxygen activity at a minimum, the least stable product, nitride, is located (when it forms). The intermediate stability phase Cr_7C_3 is found in the middle regions of the scale. The formation of the lower stability phases implies an ability of the secondary oxidants to penetrate the Cr_2O_3. Schematic activity profiles for these cases are shown in Fig. 4.9.

The thermodynamic analysis leaves many questions unanswered. Most obviously, the reason for the development of an inner Cr_2N layer in air and $CO/CO_2/N_2$ but not in $H_2/H_2O/N_2$ gas is not revealed. The a_o/a_N values of the two are almost identical and the thermodynamic driving forces for oxide and nitride formation are the same in each gas. The difference is one of reaction kinetics. This raises the more general questions as to how the secondary

oxidants can penetrate the oxide layer and what the mass transfer processes are in the inner layers. These questions are considered in Section 4.4.

4.3.2 Scaling of Chromium in Oxidising-Sulphidising-Carburising Gases

The Cr-O-S phase diagram is shown in Fig. 4.9. In all gas mixtures shown, the oxide is stable with respect to sulphide. The appearance of chromium sulphide at the scale-gas interface (Fig. 4.4C) thus demonstrates that the scale surface was not at equilibrium with the bulk gas composition.

Carbide grew beneath the oxide developed in the gas, just as in the sulphur-free gases. However, no nitride ever formed in the SO_2 containing gases, although it did in sulphur-free $CO/CO_2/N_2$. Clearly this complex pattern of behaviour cannot be predicted from the thermochemical diagrams.

4.3.3 Scaling of Iron in Oxidising-Sulphidising Gases

The Fe-S-O phase diagram is shown in Fig. 4.11, with a number of different gas compositions marked on it. These compositions were controlled using $CO/CO_2/SO_2/N_2$ mixtures. In the more commonly reported experiments, a gas of pure SO_2 or SO_2 diluted with N_2 or Ar is used. In this case, the sulphur and oxygen pressures are given by the equilibrium Eq. [4.3] plus the stoichiometric requirement $p_{S_2} = \frac{1}{2}p_{O_2}$. More generally, values corresponding to $p_{SO_2} = 7.9 \times 10^{-2}$ atm are marked on Fig. 4.11.

The Fe-S-O diagram reveals that scales in equilibrium with pure SO_2 at 1 atm should consist of oxide only at the scale-gas interface. This prediction is in fact borne out [9,10], at least in the long term, when the reaction products had the appearance of the scale in Fig. 4.1B. However, scales grown in diluted SO_2 varied in their phase constitution with p_{SO_2}. At $p_{SO_2} = 7.9 \times 10^{-2}$ atm, the scale had the same appearance as at $p_{SO_2} = 1$ atm. At lower p_{SO_2} values, scales were two-phase lamellar mixtures of oxide and sulphide [9,14]. Gases corresponding to points 7 and 8 $\left(p_{SO_2} = 2 \times 10^{-4} \text{ atm}\right)$ corroded iron to produce the scale shown in Fig. 4.1A.

Evidently, local equilibrium at the scale-gas interface might be achieved at high p_{SO_2} values, but not at low values, where sulphide apparently can exist despite the fact it is in contact with a gas in which the reaction

$$FeS + \frac{1}{2}O_2 = FeO + \frac{1}{2}S_2 \qquad [4.7]$$

is thermodynamically favoured. Furthermore, sulphide has been found to form in gases 7 and 9, which contain equilibrium p_{S_2} values below the minimum necessary for FeS formation.

Similar difficulties have been found in the much-studied Ni-S-O system, which is now briefly reviewed.

4.3.4 Scaling of Nickel in Oxidising-Sulphidising Gases

The Ni-O-S phase diagram is shown in Fig. 4.12 for T = 600°C. The point labelled X represents the equilibrium oxygen and sulphur potentials in pure SO_2 at 1 atm. It is clear that the only nickel reaction product stable in contact with this gas is the oxide. However, the experimental findings do not conform with this prediction.

The reaction of nickel with pure SO_2 in the temperature range 500−1100°C almost always produces a scale consisting of an inner layer of single-phase sulphide surmounted by a thick layer of duplex NiO + nickel sulphide mixture [8,15−17,33−36]. The inner sulphide is the one stable in equilibrium with nickel: Ni_3S_2 for T < 533°C, $Ni_{3\pm\delta}S_2$ for 533 < T < 637°C and Ni-S liquid at higher temperatures. The phase $Ni_{3\pm\delta}S_2$ ranges in stoichiometry from metal deficit to metal excess (Fig. 3.4A). The sulphide in the duplex layer formed at about 600°C has been identified as $Ni_{3\pm\delta}S_2$ [17,34], but that found in scales grown at higher temperatures has not been directly identified. Scales grown in SO_2/argon mixtures [17,34,35] had the same morphologies. The only exceptions to this pattern are the observations of a scale of NiO only at 1000°C and $p_{SO_2} = 0.01$ atm [16], and at the same temperature in an SO_2-50% Ar mixture [38].

The detailed morphology of the duplex layer varies with temperature. The concentration of sulphur in the inner part of this layer is very low at T < 525°C [37], while at around 600°C, it is lower than in the outer part of the layer [17,33]. At these lower temperatures, the sulphide precipitates in the outer part of the duplex layer are large and irregular [15,37], and because of their shape (Fig. 4.2), were described as 'flames'. As the temperature increases, the flames are replaced by a finer distribution. A duplex layer grown at 603°C was found to have a high electrical conductivity at room temperature, suggesting the presence of a continuous path made up of the metallic conductor $Ni_{3\pm\delta}S_2$ within the oxide matrix [17]. At higher temperatures, 700−800°C, the duplex scale morphology is quite complex, reflecting a tendency for the liquid sulphide to be extruded from the inner region to form protrusions at the scale-gas interface where they are subsequently oxidised [16,33]. At still higher temperatures, the overall sulphur content of the duplex layer is much reduced, and the sulphide particles are coarser and more isolated [15,33,37].

The kinetics of a nickel reaction with pure and diluted SO_2 are correspondingly complex, as shown in Fig. 4.13. Rapid rates correspond to the existence of a continuous sulphide network in the two-phase layer, and slow kinetics are observed when the sulphide content of the layer becomes small. The high diffusion coefficient of the sulphide explains these observations [17]: an interconnected sulphide network provides a continuous rapid mass transfer medium, whereas a discontinuous distribution contributes much less to mass transfer. Reaction kinetics in the temperature range 600−800°C, where sulphide-rich layers grow, have been described as linear [16,37], protective [15]

or irregular [36,39]. Linear rate constants were reported [16,34] to be approximately proportional to p_{SO_2}. In SO_2/Ar mixtures, the kinetics at 603°C showed an initial linear stage, a second stage of increasing rate, and were finally parabolic [17]. Complex kinetics in SO_2/Ar were also reported by Wootton and Birks [37].

The reaction of nickel in SO_2/O_2 gas mixtures conducted at $T < 637$°C to avoid liquid sulphide formation, led to closely similar structures: an inner layer of single-phase sulphide, and an outer oxide-plus-sulphide mixed layer [8,39–45] except when the gas was strongly oxidising, and only a small amount of sulphide formed at the scale-metal interface [8,44]. After extended periods of reaction, the scale layers started to separate, and the outer layer was converted to NiO. When separation became extensive, and nickel mass transfer was interrupted, the reaction essentially stopped and a thin outermost layer of $NiSO_4$ was formed [43].

The SO_2/O_2 reaction with nickel follows kinetics which are initially linear and then parabolic until the onset of scale separation [43]. Other investigators [37,40,41] have described the kinetics as approximately parabolic. For so long as the duplex scale is produced, its growth rate is independent of p_{O_2} and p_{SO_2}, but decreases as p_{SO_3} increases.

A schematic diffusion path is shown in Fig. 4.12 for a duplex oxide-plus-sulphide outer scale layer and $Ni_{3\pm\delta}S_2$ inner layer. Whilst showing clearly that the phase diagram provides no predictive capacity in dealing with the $Ni + SO_2$ reaction, it serves to identify the problems confronting us in understanding the scale morphology. Firstly, what are the scale-gas interaction processes which apparently permit sulphide to exist in contact with a gas which is oxidising to sulphide? Secondly, what are the processes within the scale which constrain the diffusion path to lie along the oxide-sulphide phase boundary? Thirdly, how does the inner sulphide layer form? We consider the scale-gas interactions first.

4.4 SCALE-GAS INTERACTIONS

It can usually be assumed that the bulk gas has been catalysed and brought to equilibrium with respect to the otherwise slow reactions Eqs [4.3] and [4.6]. However, this does not mean that the gas has its equilibrium composition at the scale surface. If a minority species such as SO_3 or O_2 is a reactant, then it will be consumed at the sample surface. In the absence of a catalyst at this location, the SO_3 or O_2 cannot be replenished from the gas phase, and its activity is consequently lower than the equilibrium value. The question of just what the reactant species are is seen to be important.

4.4.1 Identity of Reactant Species

The idea of slow transport within the gas coupled with rapid selective removal of some gas species into the scale leading to a different gas composition at the

TABLE 4.3 Partial Pressures and Mass Transfer Fluxes in SO_2 Gases (800°C)

	Equilibrium Composition (atm)			Fluxes (g cm^{-2} min^{-1})		
Gas	p_{SO_2}	p_{O_2}	p_{S_2}	J_{SO_2}	J_{O_2}	J_{S_2}
SO_2	1	7.3×10^{-10}	3.6×10^{-10}	3.2×10^{-2}	6×10^{-12}	5×10^{-12}
Ar-7.9% SO_2	0.079	1.3×10^{-10}	6.5×10^{-11}	2.5×10^{-3}	1×10^{-12}	1×10^{-13}

interface was proposed by Birks [9,46] to explain the formation of both oxide and sulphide at the scale surface under conditions where the sulphide is not stable. It was proposed that reaction of metal at a high activity reduced the local oxygen activity in the gas to the equilibrium value with respect to oxide formation, a very low value. As a result, the sulphur activity would rise through readjustment to maintain the SO_2 dissociation equilibrium Eq. [4.3], thereby stabilising the sulphide. Whilst qualitatively appealing, the mechanism fails quantitatively. The low p_{O_2} values proposed (about 10^{-19} atm for the Fe-FeO equilibrium at 800°C) are simply too small to support a measurable oxidation rate.

The concept of gas-phase depletion is nonetheless correct and likely to succeed when applied to less dilute species. Consider the situation in pure SO_2 and dilute Ar-SO_2. Equilibrium values of p_{S_2} and p_{O_2} at 800°C, calculated from Eq. [4.5], neglecting SO_3 formation, are shown in Table 4.3. Fluxes of the various gas species to a sample surface can be calculated for the viscous flow regime (Section 2.9). Taking representative values for laboratory experiments of sample length 1 cm and gas flow rate 0.5 m/min, we calculate the molecular fluxes shown in Table 4.3. A comparison of these values with measured weight uptake rates during corrosion in SO_2 gases is revealing.

The weight uptake rates in Table 4.4 correspond to two-phase oxide and sulphide growth on nickel (Fig. 4.2), chromium (Fig. 4.4) and cobalt, and to single-phase oxide outer layer growth on iron (Fig. 4.1B). In all cases, the measured rates far exceed the calculated fluxes of molecular oxygen and/or sulphur. It could be concluded on this basis that the reactant species was SO_2 and not oxygen or sulphur. However, it might be argued that catalysis of reaction [4.3] by the scale surface itself, if it occurred, could rapidly replenish gaseous sulphur and oxygen which could, therefore, act as the real reactants. The question has been resolved experimentally in the cases of iron and manganese.

Gas mixtures of $CO/CO_2/SO_2/N_2$ have been used [20,48,49] to independently control two of the three variables of interact $(p_{S_2}, p_{O_2}, \text{and } p_{SO_2})$, the third being set by the equilibrium Eq. [4.5]. Referring to Fig. 4.11, it is seen that gases 4–6, 9 and 10 all fall very close to the dashed line corresponding to

TABLE 4.4 Scaling Rates in SO_2 at 800°C

Metal	p_{SO_2} (atm)	Scale Surface	Kinetics	Weight Uptake Rate After 1 h (mg cm^{-2} min^{-1})	References
Ni	1	Oxide + Sulphide (l)	Linear	1.0	[31]
Co	1	Oxide + Sulphide	Parabolic	0.2	[47]
Fe	0.2	Oxide	Parabolic	0.015	[9]
	0.01	Oxide + Sulphide	Linear	1.5	[9]
Cr[a]	0.04	Oxide + Sulphide	Parabolic	0.6	[28]

[a] *In $CO/CO_2/SO_2$.*

$p_{SO_2} = 0.079$ atm. Reaction of iron with all of these catalysed gases led to the same results: an initially two-phase oxide and sulphide reaction product which was overgrown with oxide at extended times. This evolution of structure is illustrated in Fig. 4.14. Reaction kinetics were, in all cases, parabolic after an initial period of more rapid reaction. Typical data are shown in Fig. 4.15. At this temperature and p_{SO_2} value, the kinetics of a reaction with catalysed gas became parabolic after about 36 min, when the outer oxide layer was established. The parabolic rate constants corresponding to oxide growth were 3.2 ± 0.7 mg^2 cm^{-4} min^{-1} for all gases. Thus all gases produced the same reaction products at the same rate, despite the fact that p_{S_2} varied from 10^{-10} to 10^{-3} atm and p_{O_2} from 10^{-13} to 10^{-11} atm. It is therefore concluded that SO_2 was the reactant.

Further support for this conclusion is provided by the results of a reaction with gases 1, 5 and 8. These all involve essentially the same value of $p_{S_2} = 10^{-6}$ atm, but vastly different levels of p_{SO_2} and p_{O_2}. Experiment 1 led to a complex, four-layered sulphide and oxide scale which grew according to slow parabolic kinetics. Experiment 8 led to a lamellar two-phase scale (Fig. 4.1A) which grew according to rapid parabolic kinetics with $k_p = 7.8$ mg^2 cm^{-4} min^{-1}. This variation in product morphology and growth rate demonstrates that the gaseous sulphur activity was not the controlling factor. Similarly, experiments 6 and 7 were carried out at the same $p_{O_2} = 10^{-11}$ atm, but different p_{SO_2} and p_{S_2} levels. Whereas experiment 6 produced the oxide overgrowth shown in Fig. 4.1B, experiment 7 led to the lamellar structure of Fig. 4.1A and linear, rather than parabolic kinetics. Clearly the gas-phase oxygen activity was not the important factor.

In only one case, experiment 3, was SO_2 not the reactant species. In this case the equilibrium value of $p_{S_2} = 8.6 \times 10^{-2}$ atm was even higher than the

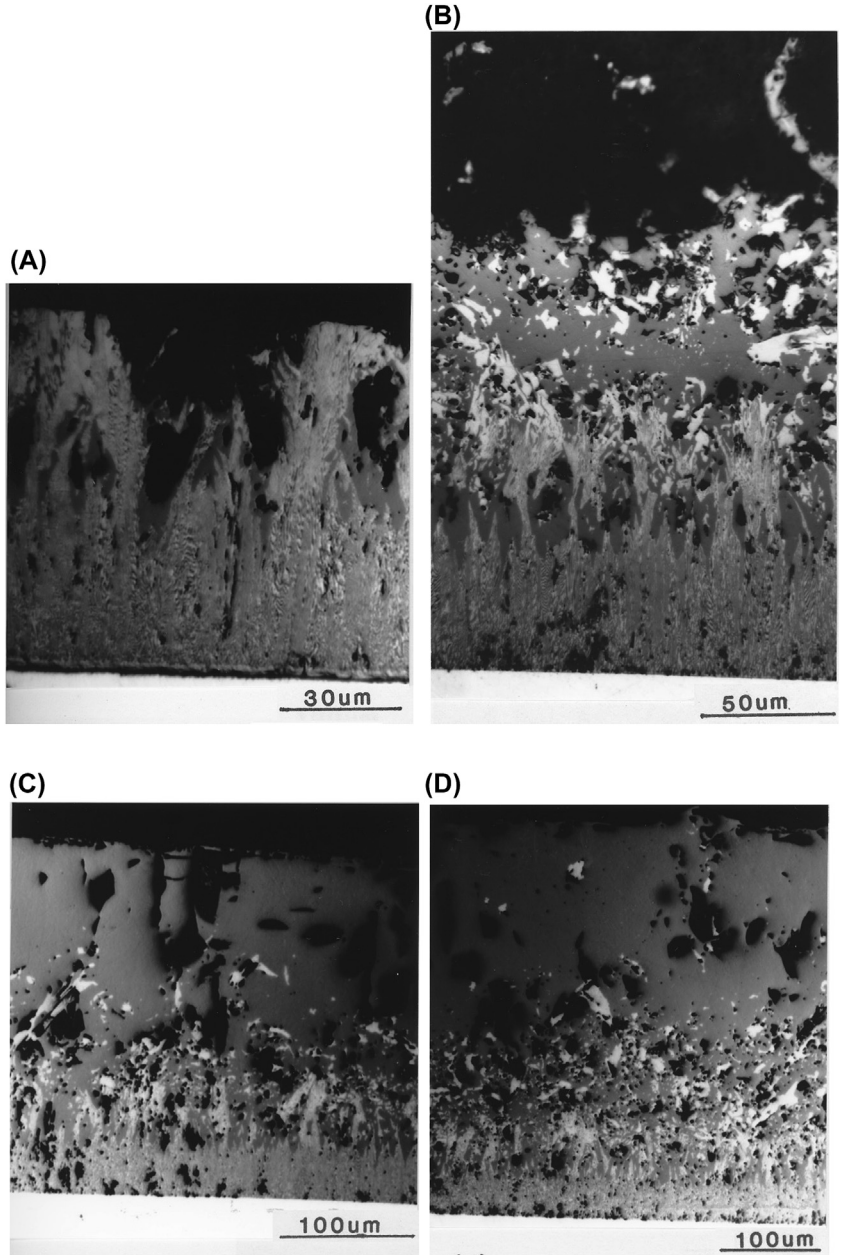

FIGURE 4.14 Evolution of sulphide-oxide scales on Fe in catalysed gas 5 (Fig. 4.11). (A) 4 min; (B) 36 min; (C) 144 min; (D) 400 min. *With kind permission from G. McAdam, D.J. Young, Oxid. Met. 37 (1992) 281, Springer Science and Business Media.*

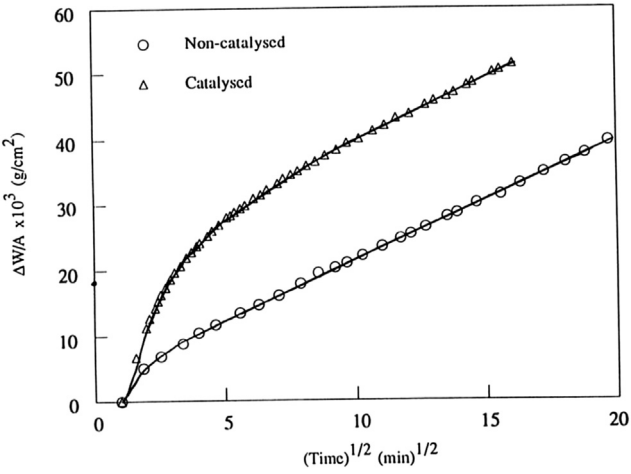

FIGURE 4.15 Kinetics of Fe reaction with gas 5 of Fig. 4.11, illustrating the effect of gas-phase catalysis. *With kind permission from G. McAdam, D.J. Young, Oxid. Met. 37 (1992) 281, Springer Science and Business Media.*

equilibrium $p_{SO_2} = 1.2 \times 10^{-2}$ atm. The reaction product was almost pure FeS, which grew according to rapid parabolic kinetics, with $k_p = 5 \times 10^{-3}$ g^2 cm^{-4} min^{-1}, a rate which could be sustained by the high partial pressure of molecular sulphur. Thus the SO_2 species ceases to be the important reactant only when its partial pressure is significantly exceeded by that of another chemically reactive species.

4.4.2 Rate Determining Processes in SO_2 Reactions

The possibility of gas-phase mass transport being the rate controlling process was considered briefly above. It was recognised that the high stability of SO_2 (g) with respect to O_2 (g) and S_2 (g) means that the latter species are necessarily in the minority. As seen in Table 4.3, the rates at which they reach a reacting sample surface are negligibly small and cannot support observed reaction rates. However, in dilute SO_2 gas mixtures, the rate at which the SO_2 species diffuses to the surface is, at 800°C, in order of magnitude similar to the scaling weight uptake rates reported in Table 4.4 for one hour of reaction. In the case of parabolic kinetics, corrosion rates would be faster at earlier times and, at some point, too high for the gas-phase process to keep up. At short times then, linear rates controlled by gaseous diffusion are predicted. Such a situation was reported by Birks [9,46] and Rahmel [11] and later confirmed by Kurokawa et al. [10] in the case of iron reaction with SO_2 gases. It was shown that the linear rate constant for mixed sulphide-plus-oxide scale growth on iron was proportional to both the flow rate of an SO_2/Ar gas mixture and its p_{SO_2}

value. As seen in the equations for viscous flow mass transfer [2.157] and [2.158], these are almost the dependencies expected for a rate controlled by gas-phase transfer. The gas mixtures used in these experiments were such that, at equilibrium, oxide was stable with respect to sulphide. Mixed oxide-sulphide scales grown in gas mixtures where, at equilibrium, sulphide was stable with respect to oxide, have also been shown [50] to thicken according to linear kinetics, attributed to gas-phase mass transfer control. In these latter experiments, the gas mixtures were based on $CO/CO_2/COS$, containing rather high p_{COS} values, and COS was the reactant species.

The reaction of manganese with SO_2 gas mixtures is very similar in morphological evolution to that of iron [3,20] when the gas compositions fall in the oxide stability field: an initial period of dual phase oxide-plus-sulphide scale growth is succeeded by development and thickening of an oxide outer layer. However, the kinetics of both reaction stages are parabolic, with SO_2 the dominant reactant species in both cases. Obviously, neither gaseous mass transfer nor an interfacial reaction, each of which leads to linear kinetics, could be involved. Instead, it must be concluded that both stages are diffusion controlled. The way in which a solid-state diffusion controlled process can occur under nonequilibrium conditions (in which a metastable sulphide phase grows) is discussed in the Section *Production of Metastable Sulphide*.

Reactions of nickel with SO_2 gas mixtures are difficult to study because of the changes of reaction product stabilities with both temperature and gas composition. Nonetheless, it is clear that the growth rates of two-phase (oxide plus sulphide) scales are strongly dependent on p_{SO_2}. Linear kinetics are attributed [16,34] to surface reaction rate control. A similar conclusion has been reached for the growth of two-phase oxide plus sulphide scales on cobalt, based on the dependence of scaling rate on p_{SO_2} and flow rate [51,52].

To summarise, then, when SO_2 is the reactant gas species, the reaction kinetics can be controlled by (1) solid-state diffusion, leading to parabolic kinetics, (2) surface reactions leading to linear kinetics or (3) gas-phase mass transfer, also leading to linear kinetics. Parabolic kinetics can be association with either two-phase scale growth or oxide layer overgrowth. Linear kinetics appear always to be associated with a two-phase reaction product. All of these findings apply to gas compositions such that oxide is stable with respect to sulphide (although they can in some cases apply to other regimes). In order to dissect these reaction mechanisms, it is clearly necessary to understand first how reaction with SO_2 can produce a thermodynamically unstable product.

4.4.3 Production of Metastable Sulphide

As we have seen, pure SO_2, $SO_2 + O_2$ or $SO_2/CO/CO_2$ gases very commonly provide environments in which the stable reaction product is oxide. The

observation of parabolic kinetics is indicative of steady-state diffusion control in the scale, and might therefore be expected to correspond to the achievement of local equilibrium at its surfaces, and the formation of oxide in contact with the gas. However, both oxide and sulphide are commonly found at the scale surface after a reaction of nickel and cobalt with oxidising-sulphidising gases, and also for iron at short times or low p_{SO_2} values. Clearly in these cases the scale surface is not at equilibrium with the gas.

In a gas in which SO_2 is the only reactant species, possible reactions at the scale surface include

$$2M + SO_2 = 2MO + \frac{1}{2}S_2 \quad [4.8]$$

$$M + SO_2 = MS + O_2 \quad [4.9]$$

$$3M + SO_2 = 2MO + MS \quad [4.10]$$

If local equilibrium for Eqs [4.8] and [4.9] is reached, their combination is thermodynamically equivalent to the formation of oxide and sulphide from the elements at their equilibrium partial pressures. In this event, the two reactions can occur simultaneously only if the gas composition falls exactly on the oxide-sulphide equilibrium line in the stability diagram. The possibility of this occurring is remote, and, as suggested long ago [9,11,50], the direct reaction [4.10] must be considered.

Reaction [4.10] can produce a mixture of oxide and sulphide, even if one of them is not in equilibrium with the bulk gas, provided that the metal activity at the scale-gas interface, a_M^s, is larger than the equilibrium value for reaction [4.10], $a_M^{(10)}$. The latter is seen from the reaction stoichiometry to be given by

$$a_M^{(10)} = K_{10}^{-\frac{1}{3}}\left(p_{SO_2}\right)^{-\frac{1}{3}} \quad [4.11]$$

with K_{10} the equilibrium constant. Under these circumstances (which amount to a steady, although nonequilibrium, state), the unstable sulphide can form, even though not at equilibrium with the gas-phase sulphur potential. However, even though molecular oxygen and sulphur are kinetically irrelevant, equilibrium could nonetheless be achieved via destruction of the sulphide through reaction with SO_2:

$$2MS + SO_2 = 2MO + \frac{3}{2}S_2 \quad [4.12]$$

As always, the reason for failure to achieve equilibrium lies in the kinetics of the situation. The sulphide will grow and be perpetuated if the rate of reaction [4.10] exceeds that of Eq. [4.12]. If it does not, then sulphide will be eliminated, and true equilibrium is established between an oxide scale and the gas.

The metastable equilibrium Eq. [4.10] is sustained by surface activities of sulphur and oxygen which lie on the sulphide-oxide equilibrium line of the stability diagram. If the SO_2 dissociation reaction is also at equilibrium on the surface, then the surface state is defined. Consider the example of iron reacting with $p_{SO_2} = 0.079$ atm, depicted in Fig. 4.11. The intersection of the dashed line (representing $p_{O_2} p_{S_2}^{\frac{1}{2}} = 0.079 K_3$) with the oxide-sulphide phase boundary represents the supposed metastable equilibrium. It also defines the minimum value of $a_{Fe}^{(10)}$ necessary at the scale surface for this equilibrium to be sustained. If, as a result of depletion, the effective value of p_{SO_2} at the interface is less than in the surrounding gas, a steady state can nonetheless be maintained, providing that a higher a_{Fe}^{s} value is available.

There remains the significant question as to just how this remarkable metastable state is arrived at. The surface state corresponds to a higher sulphur activity, but lower oxygen activity, than in the gas. This has been explained [3,53] on the basis of selective removal of oxygen from the adsorbed layer gas into the scale. At first sight, this is difficult to accept, because it is the *simultaneous* reaction of both oxygen and sulphur we are trying to explain. We turn aside for a moment to question whether the stoichiometry of reactions like Eq. [4.10] is actually achieved. A convincing demonstration is available in the case of iron reacting with dilute $CO/CO_2/SO_2$ gases of particular compositions [49].

The scale shown in Fig. 4.16 is a lamellar mixture of FeO + FeS, with a sublayer of Fe_3O_4 + FeS near the surface. It contains a sulphide volume

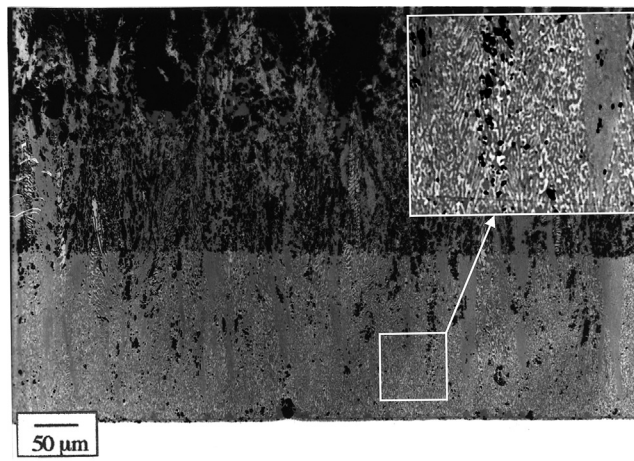

FIGURE 4.16 Scale grown on iron in $CO/CO_2/SO_2/N_2$ (gas 7 of Table 4.5) at 800°C.

fraction, f_S, measured as 0.48 ± 0.06. The reaction appropriate to the equilibrium gas composition is

$$5Fe + 2SO_2 = Fe_3O_4 + 2FeS \quad [4.13]$$

which would form sulphide and oxide in a molar ratio of 2:1. The subsequent conversion of magnetite to wüstite via the reaction within the scale:

$$Fe_3O_4 + Fe = 4FeO \quad [4.14]$$

leads to a molar ratio of 1:2 for FeS to FeO. Using standard density data, it is calculated that the resulting value of f_S would be 0.42. The good agreement of the measured value shows that, at least under the parabolic scaling conditions of this experiment, SO_2 is reacted with the stoichiometry shown in Eq. [4.13]. It should be noted for later reference that at lower p_{SO_2} values, where two-phase scales grow according to linear kinetics, the observed sulphide volume fractions are significantly lower, indicating a different mechanism.

Returning to the question of sulphur enrichment on the scale surface, we recognise that preferential sulphur adsorption will account for the observations, providing that surface concentrations are insensitive functions of activity. When kinetics are parabolic, as in the case of the scale in Fig. 4.16, the boundary conditions are fixed, and it can be assumed that SO_2 exchange between the surface and the surrounding gas is faster than SO_2 incorporation into the scale. In other words, gas adsorption is expected to approach equilibrium with respect to $SO_2(g)$, but not with the minority species $S_2(g)$ and $O_2(g)$.

Given that two solid phases are present at the scale surface, adsorption of SO_2 can be represented formally as taking place on the oxide

$$SO_2(g) + X = S\big|X + 2O_o^{\times} + 2V_M^{\times} \quad [4.15]$$

and on the sulphide

$$SO_2(g) + 2Y = 2O\big|Y + S_s^{\times} + V_M^{\times} \quad [4.16]$$

together with the surface exchange processes

$$S|X + Y = S|Y + X \quad [4.17]$$

$$O|Y + X = O|X + Y \quad [4.18]$$

Here X and Y represent surface adsorption sites on the oxide and sulphide, respectively, and cation vacancies have been assumed neutral for the sake of simplicity. If oxygen incorporation via Eq. [4.15] is favoured over sulphur incorporation, then the adsorbed phase becomes enriched in sulphur. Such a situation, coupled with a low probability of sulphur desorption, can lead to the nonequilibrium surface activities required for simultaneous oxide and sulphide formation.

These nonequilibrium activities can exist in a situation where both oxide and sulphide grow together. The growth of each phase involves consumption

of vacancies, $V_M^{\times}$, and the incorporation of additional sulphur or oxygen. If these growth processes proceed in parallel, then the balance between adsorbed sulphur and oxygen activities is preserved. The situation is thus seen to be self-sustaining for so long as several conditions are met:

a. The value of p_{SO_2} is much greater than those of p_{S_2} and p_{O_2}.
b. The metal activity at the scale surface is no less than the minimum required for reactions such as [4.10], given by Eq. [4.11], or the equivalent for other stoichiometries.
c. The rate of reaction [4.10] producing the two-phase scale is faster than the sulphide oxidation reaction [4.12].
d. Solid-state diffusion within the scale is fast enough to satisfy requirements (b) and (c).

As already seen, simultaneous oxide and sulphide formation can be maintained for lengthy times, and large extents of reaction, in the case of nickel and cobalt. In the case of iron, the two-phase product is quickly overgrown by oxide at high p_{SO_2} values, but continues for long times at low p_{SO_2}. In the case of chromium, the two-phase oxide and sulphide product grows for long times at relatively high p_{SO_2} and not at all at low p_{SO_2}.

A special situation arises when the gas composition lies in the sulphate stability field. In this case, the formation of oxide and sulphide at or close to the scale surface can be explained either by the mechanism described above, or by assuming the formation of an outer layer of metal sulphate:

$$M + SO_3 + \frac{1}{2}O_2 = MSO_4 \qquad [4.19]$$

A two-phase scale could then form beneath the sulphate layer through the reaction

$$4M + MSO_4 = MS + 4MO \qquad [4.20]$$

This mechanism was originally suggested by Alcock et al. [39] and was subsequently adopted by Kofstad and co-workers [44,45] in describing the nickel reaction. In that reaction, the two-phase product was found to be $Ni_3S_2 + NiO$ at about 600°C.

Reference to Fig. 4.12 reveals a difficulty in that the sulphate phase field is seen not to contact the observed Ni_3S_2 area. A detailed consideration of possible metastable diffusion paths has been provided by Gesmundo et al. [14]. These are based on the supposition that kinetic hindrances exist for the formation of, eg, a single-phase NiO layer, which the phase diagram predicts would develop between $NiSO_4$ and Ni_3S_2 if no other sulphide formed. Of necessity, these possibilities remain speculative.

Considerable effort has been expended [32,33,43,54] in seeking to determine whether the sulphate mechanism actually operates. At 603°C, sulphate formed only when the two-phase layer separated from the metal, so that the

nickel flux was greatly reduced and scale-gas equilibrium perhaps more closely approached. At higher temperatures, however, small amounts of sulphate were found in the absence of major scale separation. The sulphate was present as thin (<1 μm), scattered islands [38,44,45] on the surface. At 603°C, the rate decreased as p_{SO_3} increased (and p_{SO_2} decreased), indicating that the SO_2 was the reactant species. In view of the apparently marginal kinetic stability of the sulphate phase, it is uncertain whether Eq. [4.19] together with

$$9Ni + 2NiSO_4 = Ni_3S_2 + 8NiO \qquad [4.21]$$

or the direct reaction

$$\frac{9}{2}Ni + SO_3 = \frac{1}{2}Ni_3S_2 + 3NiO \qquad [4.22]$$

is more important. Both would increase in rate with p_{SO_3}, as observed experimentally. Slightly different volume fractions of sulphide and oxide are predicted from the two stoichiometries, $f_S = 0.38$ for Eq. [4.22] and 0.31 for Eq. [4.21]. The direct reaction with SO_2

$$7Ni + 2SO_2 = Ni_3S_2 + 4NiO \qquad [4.23]$$

would produce $f_S = 0.48$, a distinctly higher value. The question of relative amounts of sulphide and oxide appears not to have been investigated.

4.4.4 Independent Oxide and Sulphide Growth in SO_2

Most discussions of SO_2 corrosion are based on the occurrence of reactions such as Eq. [4.10] providing the explanation for the simultaneous formation of both oxide and sulphide. As we have seen, this is equivalent to the development of a metastable surface state which is supersaturated with respect to sulphur. If such a state develops, there seems no reason why sulphide and oxide cannot form independently via reactions such as Eqs [4.8] and [4.9].

This does in fact occur during the reaction of iron in $CO/CO_2/SO_2/N_2$ gas mixtures at 800°C, if the SO_2 partial pressure is low [49]. Catalysed gas mixtures with the equilibrium compositions shown in Table 4.5 produced scales with the morphologies shown in Fig. 4.17. It is clear that both the sulphide volume fraction and lamellar spacing, λ, varied with gas compositions. Measured values are listed in Table 4.6, along with scaling rates and phase constitutions of the scale surfaces.

At $p_{SO_2} = 2.2 \times 10^{-22}$ atm, the two-phase product was overgrown with oxide. Two-stage parabolic kinetics were observed (Fig. 4.18) with the second stage $k_w = 1.6$ mg cm^{-2} min$^{-1/2}$. This rate is in reasonable agreement with the value of 1.8 mg cm^{-2} min$^{-1/2}$ reported [55] for iron oxidation in pure oxygen at 800°C. In both experiments the bulk of the oxide is FeO, under thin external layers of Fe_3O_4 and Fe_2O_3, and the growth kinetics will therefore reflect largely the accumulation of wüstite. The diffusional flux responsible for

TABLE 4.5 Equilibrium Gas Compositions (p/atm) Used in FeS Volume Fraction Study at 800°C [49]

Gas	p_{N_2}	p_{CO_2}	p_{CO}	p_{SO_2}	p_{S_2}	p_{O_2}
1	0.12	0.88	5.3×10^{-4}	2.2×10^{-5}	1.2×10^{-13}	1.0×10^{-12}
2	0.12	0.88	1.7×10^{-4}	2.2×10^{-5}	1.2×10^{-15}	1.0×10^{-11}
3	0.12	0.88	5.3×10^{-4}	2.2×10^{-4}	1.2×10^{-11}	1.0×10^{-12}
4	0.12	0.88	1.7×10^{-4}	2.2×10^{-4}	1.3×10^{-13}	1.0×10^{-11}
5	0.24	0.76	4.6×10^{-5}	2.2×10^{-4}	1.2×10^{-15}	1.0×10^{-10}
6	0.26	0.73	4.4×10^{-5}	2.2×10^{-2}	1.2×10^{-11}	1.0×10^{-10}
7	0.24	0.76	4.6×10^{-5}	2.2×10^{-3}	1.2×10^{-13}	1.0×10^{-10}
8	0.24	0.76	1.5×10^{-4}	2.2×10^{-3}	1.2×10^{-11}	1.0×10^{-11}
9	0.12	0.88	2.3×10^{-4}	1.2×10^{-4}	1.2×10^{-13}	5.5×10^{-12}
10	0.12	0.88	3.0×10^{-4}	3.5×10^{-4}	3.2×10^{-12}	3.2×10^{-12}
11	0.12	0.88	9.5×10^{-5}	6.9×10^{-5}	1.2×10^{-15}	3.2×10^{-12}

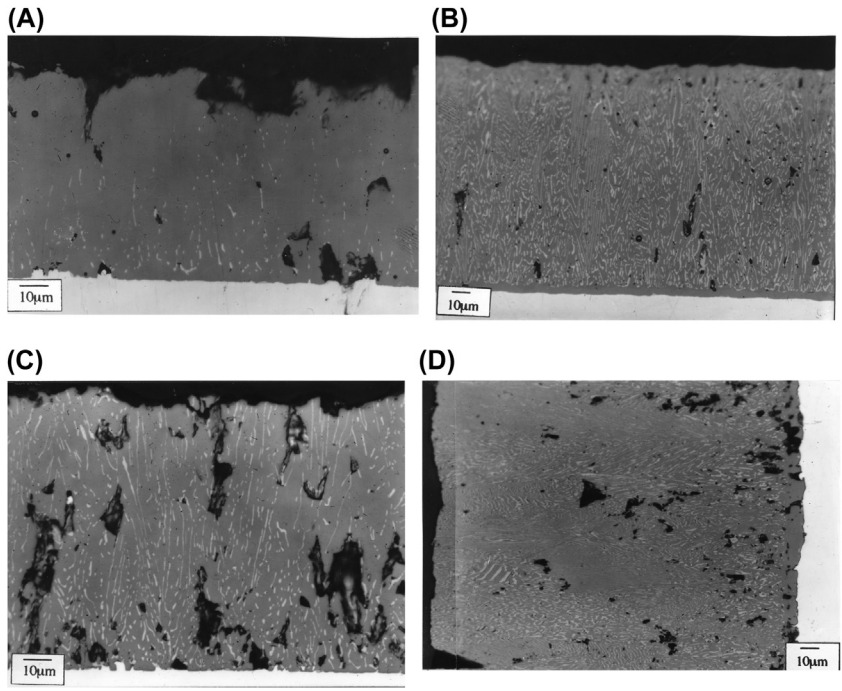

FIGURE 4.17 Scales grown on iron in $CO/CO_2/SO_2/N_2$ gas mixtures 1, 5, 9 and 10 of Table 4.5. *With kind permission from J. Unsworth, D.J. Young, Oxid. Met. 60 (2003) 447, Springer Science and Business Media.*

TABLE 4.6 Iron Oxide + Sulphide Scale Constitutions and Growth Rates, 800°C [49]

Gas	k_w (mg cm^{-2} min$^{-1/2}$)	k_1 (mg cm^{-2} min^{-1})	Phases at Surface	f_S	λ (μm)
1		0.035	FeO/FeS	0.08 ± 0.02	8
2	1.0		Fe_3O_4	0.03 ± 0.02	
3		0.063	FeO/FeS	0.13 ± 0.05	2.7
4		0.064	FeO/FeS	0.17 ± 0.04	2.4
5		0.064	Fe_3O_4/FeS	0.40 ± 0.05	2.5
6	5.2, 1.6		Fe_2O_3/Fe_3O_4		
7	4.15		Fe_3O_4/FeS	0.48 ± 0.06	<1
8	4.51		Fe_2O_3/FeS	0.36 ± 0.09	<1
9		0.054	FeO/FeS	0.21 ± 0.06	3.6
10		0.102	Fe_3O_4/FeS	0.32 ± 0.11	<1
11		0.046	FeO/FeS	0.18 ± 0.06	3.4

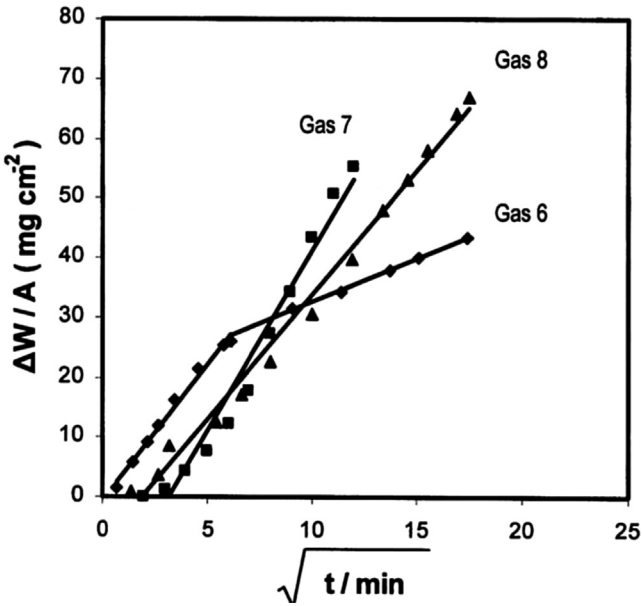

FIGURE 4.18 Parabolic scaling kinetics for iron exposed to $CO/CO_2/SO_2/N_2$ gases (Table 4.5) at 800°C ($7 \rightarrow 2.2 \times 10^{-3}$, $8 \rightarrow 2.2 \times 10^{-3}$, $6 \rightarrow 2.2 \times 10^{-2}$). *With kind permission from J. Unsworth, D.J. Young, Oxid. Met. 60 (2003) 447, Springer Science and Business Media.*

the growth of this layer is determined by the boundary conditions at its inner and outer solid−solid interfaces and is therefore independent of gas composition. Thus at high SO_2 partial pressures the reaction is ultimately one of oxidation only [9,10,50,57].

At $p_{SO_2} = 2.2 \times 10^{-3}$ atm, rapid parabolic kinetics (Fig. 4.18) accompanied the formation of a lamellar oxide and sulphide scale (Fig. 4.16). The sulphide volume fractions (Table 4.6) are in good agreement with the value $f_S = 0.42$ calculated earlier for stoichiometric uptake of SO_2 via reactions [4.13] and [4.14]. Thus a direct reaction with SO_2 produced a metastable surface state, providing a fixed boundary condition, so that diffusion controlled parabolic kinetics resulted. The reason for the more rapid rate is discussed in the next section.

At low p_{SO_2} values in the range 2.2×10^{-5} to 3.5×10^{-4} atm, two-phase oxide and sulphide scales grew according to linear kinetics. Although the value of p_{SO_2} in Gases 3, 4 and 5 was 10 times higher than in Gas 1, the rate was increased less than two-fold. Accordingly, it can be concluded that gas-phase mass transfer, which is proportional to p_{SO_2}, was not in effect. The reaction must therefore have been controlled by a surface process, but this was not Eq. [4.10] or Eq. [4.13], as shown by the diverse values of the sulphide volume fraction f_S (Table 4.6).

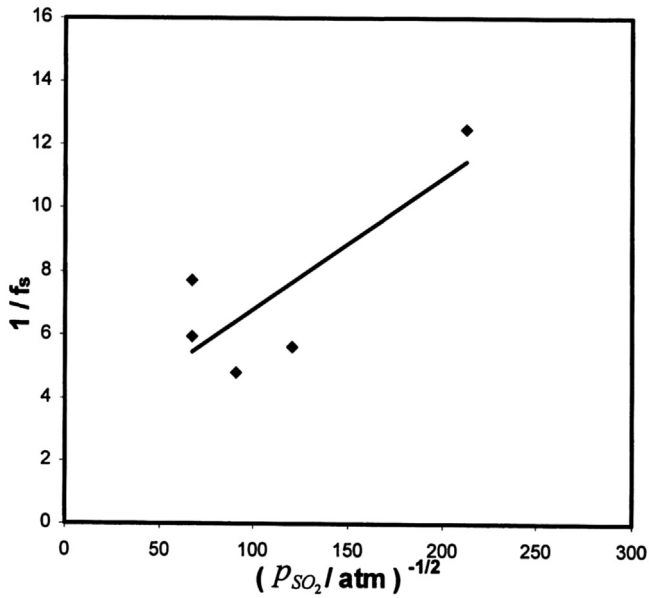

FIGURE 4.19 Variation in scale sulphide volume fraction with p_{SO_2} for (FeO + FeS) scales. *With kind permission from J. Unsworth, D.J. Young, Oxid. Met. 60 (2003) 447, Springer Science and Business Media.*

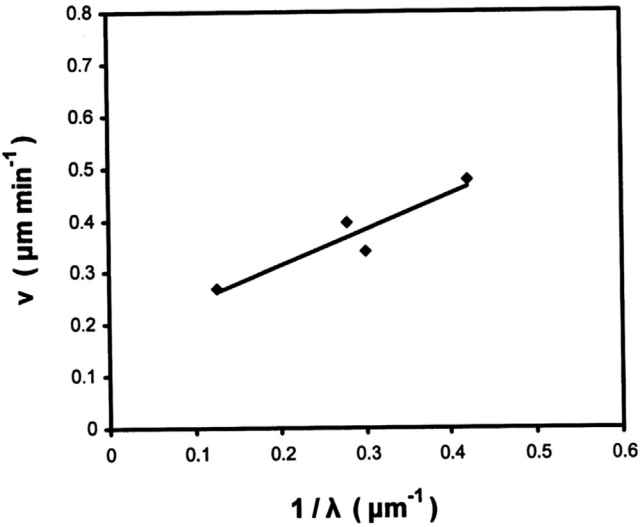

FIGURE 4.20 Variation of lamellar spacing with scale surface growth velocity for (FeO + FeS) scales. *With kind permission from J. Unsworth, D.J. Young, Oxid. Met. 60 (2003) 447, Springer Science and Business Media.*

Assuming that iron was delivered to the scale-gas interface by rapid diffusion in a process which did not control the rate, but instead led to a steady-state surface iron activity, the accumulation rates of FeO and FeS may be written from Eqs [4.8] and [4.9] as

$$\frac{dn_{\mathrm{FeS}}}{dt} = k_8 p_{\mathrm{SO_2}} \qquad [4.24]$$

$$\frac{dn_{\mathrm{FeO}}}{dt} = k_9 p_{\mathrm{SO_2}}^{\frac{1}{2}} \qquad [4.25]$$

and for time-independent rates

$$\frac{1}{N_{\mathrm{FeS}}} = 1 + \frac{k_9}{k_8}\frac{1}{p_{\mathrm{SO_2}}^{\frac{1}{2}}} \qquad [4.26]$$

Here n denotes mole number and N mole fraction. This is expressed in terms of volume fraction, using the molar volume ratio, as

$$\frac{1}{f_{\mathrm{S}}} = 1.68 + 0.68\frac{k_9}{k_8}\frac{1}{p_{\mathrm{SO_2}}^{\frac{1}{2}}} \qquad [4.27]$$

Data for FeO/FeS scales plotted in Fig. 4.19 are seen to be in only rough agreement with this prediction. The slope implies that $k_8 \approx 2k_9$.

For the reaction to continue, iron must be available at a sufficient activity at the surface of both phases. If diffusion of iron through FeS and perhaps along

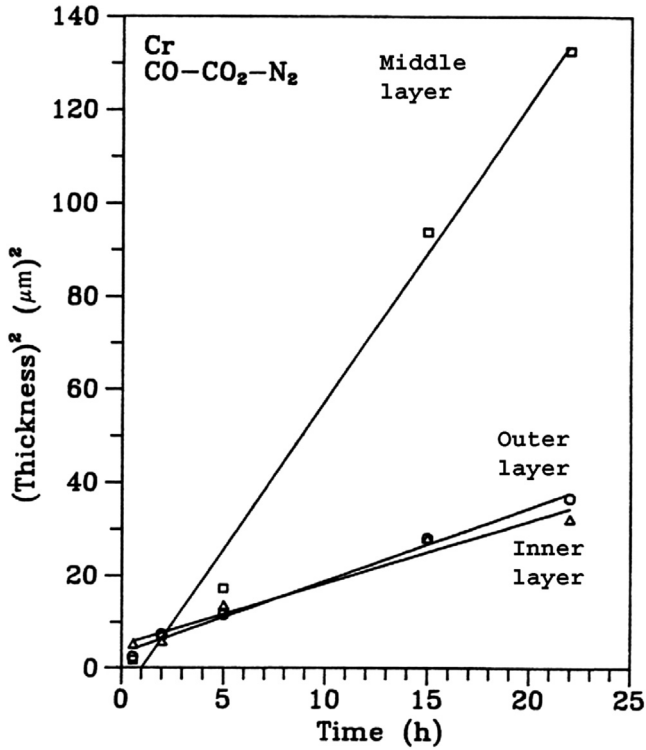

FIGURE 4.21 Kinetics of layer growth for scale shown in Fig. 4.4. *With kind permission from X.G. Zheng, D.J. Young, Oxid. Met. 42 (1994) 163, Springer Science and Business Media.*

phase boundaries predominates over diffusion through FeO, then lateral diffusion of iron must occur at the scale-gas interface in order to sustain the two-phase morphology. Treating the growth of a lamellar sulphide-oxide scale as a cellular (cooperative) phase transformation, it is recognised that the lamellar spacing, λ, would therefore be inversely dependent on scaling rate [56]. Put simply, a rapid scale growth rate allows time for only a closely spaced microstructure to develop, because of the need for lateral mass transfer on the scale surface. Conversely, when scale growth rates are relatively slow, and both gas and surface diffusion are fast, a widely spaced microstructure which lowers the overall surface energy will develop.

For a unidirectional cooperative or cellular phase transformation propagating at a velocity, v,

$$v = kD/\lambda \qquad [4.28]$$

where k is a constant which includes the driving force for reaction and D is the diffusion coefficient for lateral mass transfer on the scale surface.

If k is approximately independent of p_{SO_2}, then v varies inversely with λ at fixed temperature.

Values of v (calculated from k_l, f_S and molar volumes) are shown plotted according to Eq. [4.28] in Fig. 4.20 for FeO/FeS scales. Agreement is good in the range examined, but the relationship fails at very large lamellar spacings. In the latter case the principal phase is wüstite, the sulphide is discontinuous and the basis for Eq. [4.28] no longer exists.

It is therefore concluded that the linear kinetic regime of the Fe-SO_2 reaction is supported by two independent scale-gas reactions [4.8] and [4.9], which control the relative amounts of sulphide and oxide formed. However, the spacing of the resulting lamellar mixture of phases is controlled by delivery of the other reactant, iron, which diffuses to the surface via FeS or phase boundaries and then laterally to the reacting oxide. These results provide experimental support for the notion of a cooperative or cellular reaction hypothesised in the past [3,59].

4.5 TRANSPORT PROCESSES IN MIXED SCALES

Two very different patterns of morphological evolution have been observed: on the one hand, continued growth of multiple scale layers and on the other, accretion of different layers, reflecting successive stages of reaction. The first is illustrated by the growth of multiple layers on chromium (Fig. 4.4), the kinetics of which are seen in Fig. 4.21 to be parabolic, reflecting diffusion control. An example of the second is provided by the reaction of iron with gases containing high levels of SO_2 (Fig. 4.14). In this case, a two-phase reaction product grows in the initial reaction but is then overgrown by single-phase oxide, and no further growth of the buried oxide-plus-sulphide layer occurs. It is clear that carbon and nitrogen must penetrate the outer Cr_2O_3 scale layer in the first case, whereas this is evidently not so for sulphur in the case of iron oxide. Further information on this matter is available from preoxidation studies.

4.5.1 Effect of Preoxidation on the Reaction With Sulphidising-Oxidising Gases

Many investigations into the effect of a preformed pure oxide scale on a subsequent reaction with sulphur-containing gases have been reported. The practical aim of this work was to slow the damaging sulphidation process by using a compact, adherent oxide layer as a barrier to reaction. The results are relevant to an understanding of the transport processes involved.

Unfortunately, data for iron are limited to those of Rahmel and Gonzalez [58], who studied the reaction of preoxidised iron with $CO/CO_2/COS$ gases of high sulphur and low oxygen potential at 800 and 900°C. These gases were in the sulphide phase field and had p_{O_2} values less than the Fe/FeO equilibrium

value. A preformed FeO scale did inhibit a subsequent reaction, to an extent which increased with oxide thickness. An outer layer of FeS developed during a reaction with $CO/CO_2/COS$. Depending on gas composition, the FeS layer was in direct contact with FeO or an intermediate layer of Fe_3O_4 developed for a short time and then disappeared. The outer part of the FeO layer and the intermediate Fe_3O_4 layer developed stringers of FeS. Thus sulphur penetration of the oxide took place to only a limited extent.

Considerably more information is available for nickel. Alcock et al. [39] showed that NiO layers of submicron thickness slowed the subsequent reaction with $SO_2 + O_2$ gas but did not prevent sulphide formation. Pope and Birks [59] preoxidised nickel at $p_{O_2} = 1$ atm and 1000°C, exposing it to CO/CO_2 mixtures and finally to $CO/CO_2/SO_2$. Sulphide formed beneath the preformed oxide after an incubation period. Subsequent work [60] in which p_{SO_2} was varied led to the formation of sulphide beneath the oxide, except when p_{SO_2} was too low for reaction [4.10] to be thermodynamically possible.

Similar results were obtained by Kofstad and Akesson [61], who showed that the induction period was longer for thicker NiO scales. Worrell and Rao [32] showed that preoxidation in air at 800°C for a day to produce NiO layers of 5−10 μm provided protection against attack by SO_2 for up to 14 days.

A detailed study [62] of the effect of porosity in the initial NiO layer on subsequent corrosion in SO_2 or SO_2/O_2 was revealing. Samples with high porosity reacted with SO_2 according to rapid linear kinetics, quickly forming an inner sulphide, then filling the pores with nickel sulphide, and finally developing a two-phase product on top of the preformed oxide. Samples with low porosity reacted significantly more slowly, and those with 'extremely low' porosity reacted according to parabolic kinetics with a rate constant lower than that observed in pure oxygen. Subsequent reaction with SO_2/O_2 was different. The initial porosity was less important, because the initial NiO reacted with this gas to form a surface layer of $NiSO_4$ and then oxide and sulphide product on top of the sulphate together with sulphide channels through the underlying oxide.

Information is also available on the practically important question of chromium preoxidation. Labranche et al. [63] preoxidised chromium in H_2/H_2O gases at 900°C and exposed it immediately to $H_2/H_2O/H_2S$ atmospheres with a composition in the Cr_2O_3 stability field. No sulphide was detected after 20 h, although about 1 wt% of sulphur was found in the chromia. However, chromium sulphide was found mixed with oxide through the entire scale thickness after 111 h of reaction.

Similar results were found [64] for a reaction in $CO/CO_2/N_2$ based gases. Preoxidation at 900°C produced an adherent Cr_2O_3 layer of 3 μm thickness, with underlying sublayers containing carbide and nitride, similar to the scale shown in Fig. 4.4. Additions of SO_2 to the gas were designed to yield compositions in the Cr_2O_3 phase field, with sulphur potentials higher than the Cr/CrS equilibrium value. A reaction in these SO_2 bearing gases led to

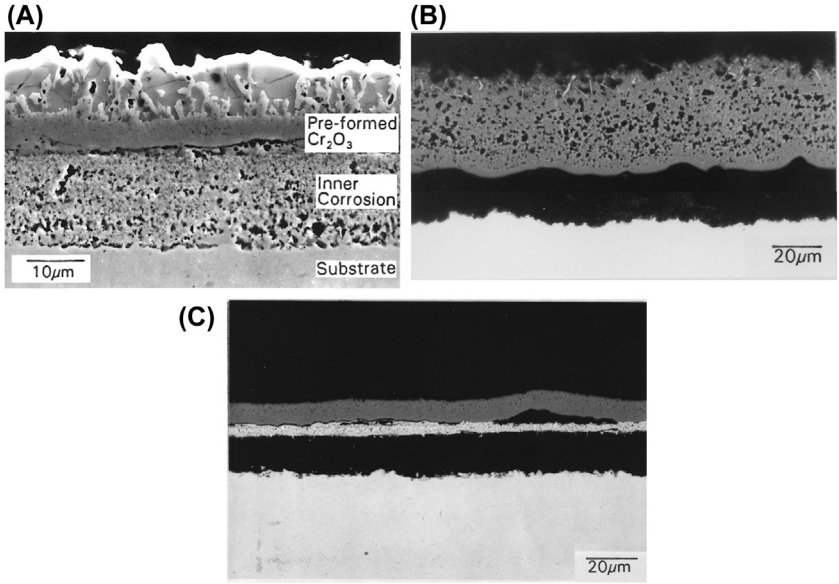

FIGURE 4.22 Scales produced on chromium by exposure at 900°C to $CO/CO_2/SO_2/N_2$ after preoxidation in $CO/CO_2/N_2$ (A) $p_{S_2} = 3 \times 10^{-7}$ atm (B) $p_{S_2} = 3 \times 10^{-8}$ atm (C) $p_{S_2} = 3 \times 10^{-9}$ atm. *Reprinted from X.G. Zheng, D.J. Young, Corros. Sci. 38 (1996) 1877, with permission from Elsevier.*

formation of a layer of $Cr_3S_4 + Cr_2O_3$ on top of the oxide (Fig. 4.22) at $p_{S_2} = 3 \times 10^{-9}$ atm and a dispersed Cr_3S_4 phase at the surface of porous Cr_2O_3 which had grown over the preformed chromia at $p_{S_2} = 3 \times 10^{-8}$ atm, while no surface sulphide formed at $p_{S_2} = 3 \times 10^{-9}$ atm. The addition of sulphur to the gas led to the disappearance of the Cr_2N layer, although the $Cr_7C_3 + Cr_2O_3$ sublayer continued to grow and incorporated particles of Cr_2N. No sulphur was found beneath the preformed oxide when $p_{S_2} = 3 \times 10^{-7}$ atm, a significant level (about 8 at %) accumulated in this region when $p_{S_2} = 3 \times 10^{-8}$ atm and less than 1% was found after a reaction at $p_{S_2} = 3 \times 10^{-9}$ atm.

It is clear that sulphur can penetrate NiO and Cr_2O_3 under at least some conditions where the oxides should be thermodynamically stable in contact with the gas in question. This problem has been discussed many times in the literature, usually in connection with sulphur transport in scales formed without preoxidation [46,51,59,60,65,66].

4.5.2 Solid-State Diffusion of Sulphur

An obvious possible method of sulphur penetration is via dissolution in and diffusion through the oxide lattice. Little information is available on either of these processes. Analytical measurements of sulphur solubility in NiO and

CoO have been reported by Pope and Birks [59], who measured maximum values at 1000°C of 0.026 wt% in NiO and 0.050 wt% in CoO.

Sulphur has been found to diffuse more rapidly than oxygen in NiO, but much slower than nickel [67–69]. In NiO single crystals, it is reported [70] that $D_S = 5.4 \times 10^{-13}\ cm^2\ s^{-1}$, $D_O = 8 \times 10^{-14}\ cm^2\ s^{-1}$ and $D_{Ni} = 10^{-11}\ cm^2\ s^{-1}$ at 1000°C. However, the combined values of sulphur solubility and diffusivity in NiO are too small to account for the sulphidation rate of nickel in mixed atmospheres [71].

In summary, there appears to be no evidence that solid-state diffusion of sulphur through metal oxide can ever account for the penetration by sulphur of preoxidised scales. On the other hand, sulphur can diffuse at significant rates in the sulphides of nickel and cobalt [16,34,39–41,72,73], thereby accounting for the inward growth of the sulphide layer which develops at the interface between these metals and their scales.

4.5.3 Gas Diffusion Through Scales

A second mode of sulphide formation beneath single-phase oxide could be via gas diffusion of sulphur or its compounds. As seen earlier (Tables 4.3 and 4.4), however, sulphur pressures in SO_2 atmospheres are generally too low to support the observed reaction rates, and the question of molecular $S_2(g)$ diffusion is therefore probably irrelevant. However, if transport occurs via the much more abundant SO_2 (or SO_3 in oxygenated gas), a viable mechanism is available.

Inward transport of sulphur by this means has been considered in detail by Birks [46,51,59,60,65], who proposed that gas compositions within scale cracks could change by reaction with the scale. Lowering the oxygen potential to values at equilibrium with the scale interior would then lead to an increase in sulphur potential through the equilibrium relationship Eq. [4.5]. In this way, sulphide formation could become thermodynamically possible within the scale. The interface between a crack surface and the gas phase is equivalent to that between the scale exterior and the gas, so the discussion provided in the section *Production of Metastable Sulphide* is equally applicable. In particular, the condition that the thermodynamically favoured reaction [4.12] be kinetically hindered applies in this situation.

Diffusion of SO_2 molecules provides a satisfactory explanation of the observations reported for a reaction of preoxidised nickel with SO_2 bearing gases. The improved resistance to sulphur penetration of a NiO scale with increased thickness and decreased porosity is an obvious consequence. Direct information on iron oxides is very limited. However, the observation during a reaction without preoxidation that the first formed oxide and sulphide layer ceases to grow once an oxide layer forms on top indicates that FeO and perhaps Fe_3O_4 are more resistant to SO_2 diffusion than NiO. The much larger grain size of FeO, and the consequently reduced availability of grain

boundaries, could be a factor. The greater plasticity of FeO and hence its lower frequency of cracking during growth could also be important in limiting the availability of pathways for molecular diffusion.

The behaviour of Cr_2O_3 scales when exposed to sulphurous gases is interestingly complex. At a high sulphur potential and high p_{SO_2}, chromium sulphide nucleated at the oxide-gas interface (Fig. 4.22). Sulphide formed at both the surface and beneath the oxide at an intermediate sulphur potential (and p_{SO_2} value), whereas at a low sulphur potential and low p_{SO_2}, some enrichment of sulphur developed beneath the oxide, but not on top. These observations are not readily understood on the basis of inward SO_2 diffusion and the diffusion path shown in Fig. 4.10.

The diffusion path illustrates the ideas first articulated by Stringer and Whittle [74] and by Stringer [75] in connection with mixed gas corrosion. In essence, it was proposed that the reduced oxygen activity within and beneath the oxide allowed an increase in a_S through the SO_2 dissociation equilibrium. The line A-X in Fig. 4.10 follows such a path. This effect, together with the relatively high chromium activity, can then stabilise the sulphide with respect to the oxide. The activity gradients for sulphur, oxygen and chromium within the two-phase layer (along the path XY) are all appropriate for its growth. A disadvantage of the description is the strong sulphur gradient within the single-phase oxide layer, along the path B-A in a direction appropriate to outward sulphur diffusion. This can be rationalised on the basis that such a process would be kinetically hindered by the low solubility of sulphur in the oxide phase. However, a more fundamental difficulty exists with the inability of the description to cope with the reaction morphology of Fig. 4.22.

This is overcome by applying again the description of a sulphur-enriched surface adsorbed layer given earlier (Eqs [4.15−4.18] in Section 4.4.3). It must be recognised that the lowering of oxygen activity relative to that of sulphur can occur both within or beneath an oxide as well as at its surface, by preferential adsorption. The line segment AX of the diffusion path in Fig. 4.10 represents both cases, providing no information on the spatial location. It thus provides no ability to predict whether sulphur enrichment occurs between an (oxide) scale surface and its interior, or between the bulk gas and an adsorbed layer. It is recognised that the diffusion path description lacks utility in this situation.

The case of preoxidised chromium reacting with SO_2 illustrates very clearly how surface processes can displace the location at which oxidant activity changes occur. The oxide shown in Fig. 4.22A was obviously gas permeable, as evidenced by the continued growth of the carbide subscale. The failure of sulphur to penetrate this material was due to its immobilisation in an outer Cr_3S_4 layer. At a lower p_{SO_2} value (Fig. 4.22B), sulphur permeated the preformed oxide more freely, because the surface sulphide formed in this gas was discontinuous. At a still lower p_{SO_2} value (Fig. 4.22C), no surface sulphide

at all was formed, and sulphur slowly permeated the oxide, enriching beneath it. Assuming that a separate sulphide phase was formed in the third gas, we see that all three cases can be described, at least in part by the diffusion path of Fig. 4.10. The differences in the path segment A-B are due to (surface) processes other than diffusion. We see that a difference arises in the case of the high p_{SO_2} gas (Fig. 4.22A) where a single-phase oxide sublayer still exists. Given the failure of equilibrium thermodynamic phase diagrams to predict scale surface constitutions in the case of SO_2 reaction, and the inability of diffusion paths to cope with surface reactions, it is reasonable to ask how predictive capacity could be arrived at. Unfortunately, only qualitative statements can be made, as will be seen in Section 4.6, *Predicting the Outcome of Mixed Gas Reactions*.

4.5.4 Scale Penetration by Multiple Gas Species

As has been experimentally demonstrated and discussed in some detail above, SO_2 molecules can both react at scale surfaces and penetrate oxides to react in the scale interior. Scales which are permeable to one gas species might be expected to transmit others, and this is indeed the case.

As seen earlier (Fig. 4.4), nitride and carbide can form beneath a Cr_2O_3 scale during exposure to mixed gases. As is clear from Fig. 4.21, carbon and nitrogen continue to penetrate the oxide layer, supporting diffusion-controlled growth of the underlying carbide and nitride layers throughout the observed reaction. Gas phase a_C and a_N values were high enough to stabilise the carbide and nitride at high a_{Cr} values, and the schematic activity profiles of Fig. 4.9 illustrate the diffusional steady-state. The exception to this pattern was the single-phase oxide scale grown in $H_2/H_2O/N_2$ gas, which was obviously not permeable to nitrogen.

It is known [76] that carbon solubility in Cr_2O_3 is negligible, and it seems likely that the same would be true of nitrogen. Neither of these species could penetrate the oxide by lattice diffusion, and molecular transport via scale imperfections is indicated. Diffusion along these imperfections must be rather slow to produce the activity gradients corresponding to the layered scales which result. Accordingly, it is proposed that the transport mechanism is one of diffusion of adsorbed gas molecules along grain boundaries or similar internal surfaces.

Competitive adsorption processes give rise to interactions among the diffusing species. Thus the nonpolar N_2 molecules are displaced by relatively strongly adsorbing H_2O, and the absence of any nitride layer underneath Cr_2O_3 grown in $H_2/H_2O/N_2$, despite its thermodynamic stability, is thereby explained. On the other hand, nitrogen is able to diffuse along these internal surfaces if the oxidant is CO_2 and the corresponding adsorbed species is CO.

As seen earlier (Section 4.3.2), addition of SO_2 to the $CO/CO_2/N_2$ gas also suppressed the expected nitride formation, even when the p_{SO_2} value was too low to form external surface sulphide. Under these circumstances, the rate of inner carbide growth was slowed, but not stopped. Obviously, these effects would not be possible if the mechanism of penetration by secondary oxidants was one of gaseous diffusion through large defects. Again, it is concluded that mass transport involved much smaller defects, such as internal surfaces. Preferential adsorption of sulphur on oxide boundaries would be expected. It seems that the more reactive CO molecule can adsorb to some extent on the sulphur-poisoned grain boundaries, whereas the unreactive N_2 cannot.

4.5.5 Metal Transport Processes

In a two-phase scale such as the examples shown in Figs 4.1A, 4.2 and 4.4C, metals can diffuse as cations in the lattices of both phases and along the boundaries between them. If these phases are continuous, in the sense of providing an unbroken diffusion pathway between metal and the scale-gas interface, then the flux of metal in each phase is described by Eq. [3.62]. However, as has become abundantly clear, the boundary conditions at the scale-gas interface are far from equilibrium, and unknown. This makes the application of Eq. [3.62] impossible. Moreover, the diffusional properties of phase boundaries such as those between oxide and sulphide, which can be so abundant, are unknown.

In the absence of basic data, it is appropriate to assess the contributions of the different diffusional processes by comparing scaling rates. Table 4.7 lists rate constants for oxidation, sulphidation and the reaction with SO_2 for several metals at particular temperatures. Most values refer to a reaction with the relevant gas at a pressure of 1 atm. The comparison is not ideal, because the p_{S_2} and p_{O_2} values in effect at a scale-SO_2 gas interface will be much less than 1 atm. However, as the effect of oxidant partial pressure on reactions involving only one species Eqs [3.76 and 3.90] is small, the values shown are sufficient for our purposes.

Corrosion in SO_2 is seen to be faster than oxidation in pure O_2 whenever a two-phase product is formed. The difference for iron and manganese is only moderate, at about an order of magnitude, because both FeO and MnO have large concentrations of defects and oxidation is, in any case, rapid. Conversely, the difference for nickel and chromium is very large. The sulphidation rates of both metals are many orders of magnitude faster than the oxidation rates, because the sulphides possess much more defective structures. The formation of a continuous sulphide phase in the scales developed by these metals therefore provides an alternative, much more rapid diffusion pathway for cations.

TABLE 4.7 Values of k_w ($g^2\ cm^{-4}\ s^{-1}$) for Reaction in O_2 (1 atm), S_2 (1 atm) and SO_2 (p Indicated)

		O_2		S_2		SO_2		
Metal	T (°C)	k_w	References	k_w	References	k_w	p (atm)	References
Fe	800	5.5×10^{-8}	[55]	8.1×10^{-6}	[77]	(a) 4×10^{-8}	2.2×10^{-2}	[49]
						(b) 3×10^{-7}	2.2×10^{-3}	[49]
Mn	800	1.6×10^{-9}	[30]	3.2×10^{-9}	[78]	(a) 3×10^{-9}	7.3×10^{-2}	[20]
						(b) 1.1×10^{-8}	2.5×10^{-4}	[20]
Ni	600	1.0×10^{-13}	[79]	9×10^{-7}	[80]	(b) 2.5×10^{-6}	1.0	[17]
Cr	900	2×10^{-13}	[81]	8×10^{-7}	[80]	(b) 1.1×10^{-8}	3.9×10^{-2}	[28]

(a) Single-phase oxide scale surface; (b) two-phase oxide + sulphide scale surface.

4.6 PREDICTING THE OUTCOME OF MIXED GAS REACTIONS

The corrosion reactions examined in this Chapter exhibit a diversity of outcomes, and an attempt to arrive at a unified view is worthwhile. As we have seen, the use of solid-gas thermodynamic equilibrium in predicting scale surface constitutions is successful in some cases (oxidation-carburisation-nitridation of chromium, sulphidation-oxidation of iron and manganese under certain condition) and is without value in other situations, notably the sulphidation-oxidation of nickel and chromium.

Among the factors leading to these different outcomes are the differing stabilities of the reaction products, the existence of heteronuclear molecules appropriate to biphase solid production and the relative rates at which secondary, metastable reaction products can be incorporated into the scale or destroyed by interaction with gas species.

Selected ΔG° values for reactions of interest are shown in Table 4.8. We consider first the question of why chromium carbide and nitride develop beneath Cr_2O_3 scale layers, but never at the surface, whereas chromium sulphide can develop at both locations. Appropriate gas molecules for simultaneous formation of two products exist in all cases: CO, NO and SO_2. However, the feasibility of the various reactions differs greatly. Firstly, the species NO is present at only very small concentrations, as can be seen from the equilibrium

$$\frac{1}{2}N_2 + \frac{1}{2}O_2 = NO, \quad \Delta G^\circ = 90{,}136 - 12.4\,T \ \left(J\,mol^{-1}\right) \qquad [4.29]$$

At 900°C, for example, a gas mixture containing $p_{N_2} = 1$ atm and $p_{O_2} = 10^{-5}$ atm has an equilibrium value $p_{NO} = 2 \times 10^{-7}$ atm. This is far too low to support a surface reaction, and the process (e) in Table 4.8 is kinetically irrelevant. The same evaluation is arrived at for other nitrogen oxides, and we conclude that no reaction is available for the formation of metastable nitride at

TABLE 4.8 Selected Mixed Gas Reaction Free Energies [82,83]

Reaction	T (°C)	ΔG°/kJ mol^{-1}
(a) $3Fe + SO_2 = FeO + 2FeS$	800	−195
(b) $\frac{7}{2}Ni + SO_2 = \frac{1}{2}Ni_3S_2 + 2NiO$	600	−92
(c) $3Cr + CO = \frac{1}{3}Cr_7C_3 + \frac{1}{3}Cr_2O_3$	900	−124
(d) $\frac{7}{3}Cr + SO_2 = CrS + \frac{2}{3}Cr_2O_3$	900	−536
(e) $\frac{8}{3}Cr + NO = Cr_2N + \frac{1}{3}Cr_2O_3$	900	−379

a Cr_2O_3 surface. Chromium nitride can only develop by inward diffusion of nitrogen to a zone where the oxygen activity is low and chromium activity high. The question of nitride formation on iron or nickel at high temperatures does not arise, as no stable compounds exist.

A similar situation exists with carbides. No nickel carbide is stable, and the iron carbide, Fe_3C, is of marginal stability. In fact, it is metastable below 748°C, where values of $a_C > 1$ are required for its formation. Whilst Fe_3C is formed on iron in strongly carburising gases (see Chapter 9), the simultaneous formation of both carbide and oxide on pure iron has not been reported. However, elemental carbon can be deposited in the inner parts of an iron oxide scale grown in CO_2 at low temperatures, around 400−500°C [84,85]. Gas molecules diffuse inwards through the oxide and the CO/CO_2 ratio alters according to

$$CO_2 = CO + \frac{1}{2}O_2 \qquad [4.30]$$

as the oxygen activity of the scale decreases towards the metal-scale interface. As p_{CO} rises, the Boudouard reaction

$$2CO = CO_2 + C \qquad [4.31]$$

becomes favoured (providing the temperature is low) and carbon deposition results. This is analogous to the formation of chromium carbide beneath a Cr_2O_3 scale, with the difference being that no iron carbide can form, and instead, graphite precipitation results. A significant volume expansion accompanies reaction [4.31], and the resulting compressive stresses lead to oxide 'bursting'.

Chromium carbides are significantly more stable (Table 2.1), and the possibility of simultaneous $Cr_7C_3 + Cr_2O_3$ formation is now considered. As seen in Table 4.8, their formation by reaction (c) with CO is thermodynamically favourable, but the driving force is rather small, at only 42 kJ mol^{-1} of chromium. The reaction

$$2Cr + 3CO_2 = Cr_2O_3 + 3CO \qquad [4.32]$$

with $\Delta G^\circ = -274$ kJ mol^{-1} at 900°C is much more favourable at gas component activities near unity. The possibility of the energy barrier to surface carbide formation being overcome by oxygen depletion and consequent carbon enrichment via

$$CO = C + \frac{1}{2}O_2 \qquad [4.33]$$

is remote. If this reaction dominated the surface (and CO_2 processes could be neglected), the situation could be represented by the line AB in Fig. 4.8. It is seen that oxygen depletion at constant p_{CO} would lead to carbon precipitation, but not to carbide formation. We therefore conclude that formation of carbide

at a Cr_2O_3 scale surface is not thermodynamically favoured. Instead, carbide can form beneath the oxide, where the oxygen activity is low and chromium activity high.

The situation is quite different when SO_2 is the reactant species, as seen in Table 4.8. The simultaneous formation of Cr_2O_3 and CrS in contact with the gas via reaction (d) is strongly favoured, with $\Delta G^\circ = -230\ \text{kJ mol}^{-1}$ of metal at $T = 900°C$ and $p_{SO_2} = 1$ atm. The alternative reaction

$$2Cr + \frac{3}{2}SO_2 = Cr_2O_3 + \frac{3}{2}S_2 \qquad [4.34]$$

has $\Delta G^\circ = -399\ \text{kJ mol}^{-1}$ at 900°C, corresponding to $-200\ \text{kJ mol}^{-1}$ of chromium at unit activity of gas components. Whilst the reaction is favoured even at low p_{S_2} values, a mechanism for sulphur enrichment on the surface (represented by the shift from A to B in Fig. 4.10) is available. The combination of a strong driving force plus a mechanism for selective adsorption makes two-phase product formation on chromium much more favoured thermodynamically in SO_2 than in CO.

As is now clear, the greater stability of metal sulphides compared to that of carbides and nitrides is the fundamental reason that metastable surface sulphide formation is sometimes possible in sulphidising-oxidising gases. The question of interest then is why in some cases the formation of two-phase scale continues for long reaction times, while in others it ceases after a short time. The situation was described earlier in terms of competing reactions for two-phase product formation Eq. [4.10] and for sulphide oxidation Eq. [4.12]. While the latter is purely a surface reaction, the former is controlled at least partially by the rate of metal transport through the scale. Thus the faster the rate of scale growth, the less likely it is that sulphide formed at the surface will be oxidised. On this basis (Table 4.7), it would be predicted that suphide formation would continue for long times in the case of nickel, but for shorter times in the case of iron, manganese and chromium. The analysis is qualitatively successful for manganese, iron and nickel, but not for chromium, and a further factor must be involved.

It has been suggested [3] that an important factor is the metal activity at the surface required for two-phase scale formation through reaction [4.10], $a_M^{(2\text{-phase})}$, relative to the activity required for true local equilibrium of reaction [4.8], $a_M^{(\text{oxide})}$. The ratio of metal activities required for these competing processes is

$$\frac{a_M^{(2\text{-phase})}}{a_M^{(\text{oxide})}} = \frac{K_8^{\frac{1}{2}}}{K_{10}^{\frac{1}{3}}} \frac{p_{SO_2}^{\frac{1}{6}}}{P_{S_2}^{\frac{1}{4}}} \qquad [4.35]$$

Thus lower values of p_{SO_2} and higher values of p_{S_2} lower the metal activity level required to form a two-phase scale rather than the oxide. The metal

activity at the scale-gas interface is high during the initial stages of reaction and presumably decreases progressively as the scale thickens, until its value is below the minimum of Eq. [4.35]. This accounts satisfactorily for the observed behaviour of iron, which forms a two-phase product for long times at low p_{SO_2} values but quickly converts to an oxide-only outer layer at high p_{SO_2}. It is also broadly consistent with observations on the chromium reaction. When reacted at $p_{SO_2} = 1$ atm, chromium formed only oxide [30], but at $p_{SO_2} = 0.04$ atm, it developed a two-phase product at the scale-gas interface [28]. However, the latter gas, when fully equilibrated, would have contained $p_{SO_2} = 10^{-10}$ atm, a value too low to be kinetically significant, but $p_{COS} = 4 \times 10^{-4}$ atm. In short, a different surface mechanism was in effect, and the utility of Eq. [4.35] cannot be tested.

The value of a_M at the scale-gas interface is certainly an important parameter. As noted by Gesmundo et al. [3], any preoxidation treatment carried out at a high p_{O_2} would result in a low surface a_M value and an inability of the scale to form any oxide-plus-sulphide product when subsequently exposed to SO_2. As seen earlier, preoxidation of nickel at high p_{O_2} (air or pure oxygen) produced scales which resisted sulphide formation at the surface and eventually formed sulphide beneath the oxide when exposed to SO_2. This is to be contrasted with the continued growth of oxide-plus-sulphide on nickel exposed to SO_2 without preoxidation, where a higher surface a_{Ni} value must have been available.

An analogous effect has been observed [64] in the reaction of chromium. As discussed earlier, chromium reacts with $CO/CO_2/N_2/SO_2$ gas mixtures to form an outer layer of $Cr_2O_3 + Cr_5S_6$. If, however, the metal was first preoxidised and then exposed to the same oxidising-sulphidising gas mixture, the sulphide formed at the scale surface was identified as Cr_3S_4. The Cr_5S_6 phase is not stable at the reaction temperature of 900°C, being formed during cooling from the high temperature $Cr_{1-\delta}S$ phase. The growth of the lower sulphide indicates that a higher surface a_{Cr} value was available. Preoxidation depressed a^s_{Cr}, allowing the higher sulphide to form.

The experimental data for both nickel and chromium provide qualitative support for the proposal that surface sulphide formation is favoured by high surface a_M values, and that these can be lowered by suitable preoxidation treatments. High surface a_M values are supported by rapid diffusion of metal through the sulphide phase, or along interphase boundaries. However, despite these successes, Eq. [4.35] is not universally applicable. Evaluation of the relevant equilibrium constants using the data in Table 4.8 leads to the prediction that formation of a two-phase product requires a higher activity of nickel than of iron. Despite this, a sulphide-plus-oxide scale persists on nickel; whereas on iron, it is soon overgrown by oxide. Here the kinetic factors outweigh the thermodynamics, because diffusion in the nickel sulphides is fast enough to maintain high a^s_{Ni} values.

As will be discussed in Chapter 7, further complexities arise in the mixed gas corrosion of alloys. It is sufficient therefore to conclude that the formation of additional reaction products (carbides, nitrides and sulphides) during oxidation of metals is governed by both thermodynamic and kinetic factors as well as gas adsorption processes.

In general, thermochemical diagrams are successful in predicting the phases formed in contact with carburising-oxidising and nitriding-oxidising gases. This success is attributable to the low stability of carbides and nitrides compared to that of oxides. On the other hand, the diagrams frequently fail to predict scale constitutions formed in contact with sulphidising-oxidising gases. One reason for this failure is the higher stability of metal sulphides, which can be sufficient to enable a metastable oxide-plus-sulphide mixture to form. Another reason is the ability of sulphur to adsorb preferentially on the scale surface, resulting in a surface richer in sulphur than the gas phase. The differences between the scales grown on different metals exposed to oxidising-sulphidising gases cannot be rationalised in terms of phase stabilities alone. The ability of the scale to support rapid metal diffusion, thereby maintaining high surface metal activities, is an important factor in promoting two-phase product formation in direct reaction with SO_2. In this respect, the behaviour of nickel is unique, as a result of its formation of high diffusivity $Ni_{3\pm\delta}S_2$ ($D_{Ni} \approx 10^{-5}$ cm^2 s^{-1} at 600°C) at temperatures of 533–635°C, and liquid sulphide at higher temperatures. For this reason, the formation of mixed oxide-plus-sulphide on nickel continues for very long times, and metal destruction is extensive.

The use of diffusion paths to describe phase distributions within reaction product scales is only sometimes of value. Inward diffusion of gaseous species adsorbed on internal surfaces can be represented by diffusion paths in the cases of oxidation-carburisation and oxidation-nitridation of chromium. However, interaction between diffusing species (eg, CO, N_2, SO_2) via competitive adsorption can prevent the diffusion of nitrogen and slow the transport of carbon, changing the diffusion paths. The diffusion path concept is of even less value in describing sulphidation-oxidation reactions. In the case of nickel and chromium, SO_2 usually reacts at the scale surface rather than penetrating the oxide. In the case of iron, SO_2 reacts at the surface initially, but cannot penetrate the iron oxide outer layer once it is formed.

A very large research effort into mixed gas corrosion reactions has yielded a substantial body of descriptive knowledge, an appreciation of the multitude of factors involved and a capacity to interpret and understand the results. However, our predictive capacity is at best qualitative. Nonetheless, the understanding which has been developed does provide a rational basis for experimental design to use in any future research. This may prove to be of considerable value as new technologies for fossil fuel processing are developed to improve efficiencies and reduce greenhouse gas emissions.

REFERENCES

[1] W.F. Chu, A. Rahmel, Rev. High Temp. Mater. 4 (1979) 139.
[2] K. Natesan, Corrosion 41 (1985) 646.
[3] F. Gesmundo, D.J. Young, S.K. Roy, High Temp. Mater. Proc. 8 (1989) 149.
[4] M.F. Stroosnijder, W.J. Quadakkers, High Temp. Technol. 4 (1986) 141.
[5] J. Stringer, in: J.D. Embury (Ed.), High Temperature Oxidation and Sulphidation Processes, Pergamon Press, New York, 1990, p. 257.
[6] W.T. Bakker, J. Stringer, Mater. High Temp. 14 (1997) 101.
[7] F.H. Stott, J.F. Norton, Mater. High Temp. 14 (1997) 132.
[8] C.S. Giggins, F.S. Pettit, Oxid. Met. 14 (1980) 363.
[9] T. Flatley, N. Birks, J.I.S.I. 209 (1971) 523.
[10] K. Kurokawa, T. Narita, K. Nishida, in: Proceedings of the 3rd JIM International Symposium on High Temperature Corrosion of Metals and Alloys, Japan Institute of Metals, Sendai, 1983, p. 465.
[11] A. Rahmel, Werkst. Korros. 23 (1972) 273.
[12] B. Chatterrjee, A.J. Dowell, Corros. Sci. 15 (1975) 639.
[13] J. Gillewicz-Wolter, Oxid. Met. 11 (1977) 81.
[14] F. Gesmundo, C. DeAsmundis, S. Merle, C. Bottino, Werkst. Korros. 30 (1979) 179.
[15] P. Barrett, B. Dupuisson, Rev. Int. Ht. Temp. Refract. 14 (1977) 145.
[16] P. Kofstad, G. Akesson, Oxid. Met. 12 (1978) 503.
[17] K.L. Luthra, W.L. Worrell, Met. Trans. A 9A (1978) 1055.
[18] B. Gillot, D. Garnier, P. Barrett, Ann. Chim. Fr. 4 (1979) 277.
[19] F. Gesmundo, C. De Asmundis, in: I. Kirman, J.B. Marriott, M. Merz, P.R. Sahm, D.P. Whittle (Eds.), Proceedings of International Conference on Behaviour of High Temperature Alloys in Aggressive Environments, Metals Society, London, 1980, p. 435.
[20] G. McAdam, D.J. Young, Oxid. Met. 37 (1992) 301.
[21] C.A. Snavely, C.L. Faust, J. Electrochem. Soc. 97 (1950) 99.
[22] V.I. Arkharov, V.N. Konev, I.S. Trakhtenberg, Phys. Met. Mettall. 5 (1957) 164.
[23] G.R. Wilms, T.W. Rea, J. Less Common Met. 1 (1959) 152.
[24] W.G. Hagel, Trans. Am. Soc. Met. 56 (1963) 583.
[25] G.R. Wilms, T.W. Rea, J. Less Common Met. 3 (1961) 234.
[26] A.U. Seybolt, D.H. Haman, Trans. Met. Soc. AIME 230 (1964) 1294.
[27] X.G. Zheng, D.J. Young, Oxid. Met. 42 (1994) 163.
[28] X.G. Zheng, D.J. Young, Corros. Sci. 36 (1994) 1999.
[29] V.N. Konev, N.G. Bogacleva, V.I. Arkarov, Fiz. Met. Metalloved. 9 (1960) 358.
[30] C. De AsMundis, F. Gesmundo, C. Bottino, Oxid. Met. 14 (1980) 351.
[31] G.J. Yurek, M.H. La Branche, in: A.V. Levy (Ed.), Proceedings of the Conference on Corrosion-Erosion Wear of Materials in Emerging Fossil Energy Systems, NACE, Houston, TX, 1982, p. p.933.
[32] X.G. Zheng, D.J. Young, Mater. Sci. Forum 251−254 (1997) 567.
[33] F. Gesmundo, C. DeAsmundis, P. Nanni, Oxid. Met. 20 (1983) 217.
[34] M. Seiersten, P. Kofstad, Corros. Sci. 22 (1982) 497.
[35] W.L. Worrell, B.K. Rao, in: R.A. Rapp (Ed.), Proceedings of the International Conference on High Temperature Corrosion, NACE, Houston, TX, 1983, p. 295.
[36] N. Jacobson, W.L. Worrell, in: G. Simkovich, V.S. Stubican (Eds.), Proceedings of the 3rd International Conference on Transport in Nonstoichiometric Compounds, Plenum Press, New York, 1984, p. 451.

[37] M.R. Wootton, N. Birks, Corros. Sci. 12 (1972) 829.
[38] H. Nakai, K. Okada, Y. Kato, in: Proceedings of the 3rd JIM International Symposium on High Temperature Corrosion of Metals and Alloys, Japan Institute of Metals, Sendai, 1983, p. 427.
[39] C.B. Alcock, M.G. Hocking, S. Zador, Corros. Sci. 9 (1969) 111.
[40] V. Vasantasree, M.G. Hocking, Corros. Sci. 16 (1976) 261.
[41] M.G. Hocking, V. Vasantasree, Corros. Sci. 16 (1976) 279.
[42] K.L. Luthra, W. Worrell, in: Z.A. Foroulis, F.S. Pettit (Eds.), Proceedings of the Symposium on Properties of High Temperature Alloys, vol. 77-1, Electrochemical Society, New York, 1977, p. 318.
[43] K.L. Luthra, W.L. Worrell, Met. Trans. A 10A (1979) 621.
[44] B. Haflan, P. Kofstad, Corros. Sci. 23 (1983) 1333.
[45] P.K. Lillerud, B. Haflan, P. Kofstad, Oxid. Met. 21 (1984) 119.
[46] N. Birks, in: S.A. Jansson, Z.A. Foroulis (Eds.), Proceedings of the Symposium on High Temperature Gas-Metal Reactions in Mixed Environments, Metal Society of AIME, New York, 1973, p. 322.
[47] K. Holthe, P. Kofstad, Corros. Sci. 20 (1980) 919.
[48] G. McAdam, D.J. Young, Oxid. Met. 37 (1992) 281.
[49] J. Unsworth, D.J. Young, Oxid. Met. 60 (2003) 447.
[50] A. Rahmel, J.A. Gonzalez, Werkst. Korros. 22 (1971) 283.
[51] P. Singh, N. Birks, Oxid. Met. 12 (1978) 23.
[52] N.S. Jacobson, W.L. Worrell, J. Electrochem. Soc. 131 (1984) 1182.
[53] P. Kofstad, High Temperature Corrosion, Elsevier, London, 1988.
[54] V. Guerra-Brady, W.L. Worrell, in: P. Barret, L.C. Dufour (Eds.), Proceedings of the 10th International Symposium on Reactivity of Solids, Materials Science Monographs, vol. 28A, Elsevier, Amsterdam, 1985, p. 61.
[55] M.H. Davies, M.T. Simnad, C.E. Birchenall, Trans. AIME 191 (1951) 889.
[56] M. Hillert (Ed.), The Mechanisms of Phase Transformations in Crystalline Solids, Institute of Metals, London, 1969.
[57] N. Birks, G. Meier, Introduction to High Temperature Oxidation of Metals, Edward Arnold, London, 1983.
[58] A. Rahmel, J.A. Gonzalez, Corros. Sci. 13 (1973) 433.
[59] M.C. Pope, N. Birks, Oxid. Met. 12 (1978) 173.
[60] P. Singh, N. Birks, Werkst. Korros. 31 (1980) 682.
[61] P. Kofstad, G. Akesson, Oxid. Met. 13 (1979) 57.
[62] W.L. Worrell, B. Ghosal, in: Proceedings of the 3rd JIM International Symposium on High Temperature Corrosion of Metals and Alloys, Japan Institute of Metals, Sendai, 1983, p. 419.
[63] M.H. La Branche, A. Garrat-Reed, G.J. Yurek, J. Electrochem. Soc. 130 (1983) 2405.
[64] X.G. Zheng, D.J. Young, Corros. Sci. 38 (1996) 1877.
[65] N. Birks, in: Z.A. Foroulis, F.S. Pettit (Eds.), Proceedings of the Symposium on Properties of High Temperature Alloys, Electrochemical Society, vol. 77-1, 1977, p. 215.
[66] K.N. Strafford, P.J. Hunt, in: R.A. Rapp (Ed.), Proceedings of the International Conference on High Temperature Corrosion, NACE, Houston, TX, 1983, p. 380.
[67] D.R. Chang, R. Nemoto, J.B. Wagner, Met. Trans. A 78A (1976) 803.
[68] W.Y. Howng, J.B. Wagner, J. Phys. Chem. Solids 39 (1978) 1019.
[69] P. Dumes, A. Fauvre, J.C. Colson, Ann. Chim. Fr. 4 (1979) 269.
[70] J.S. Choi, W.J. Moore, J. Phys. Chem. 66 (1962) 1308.

[71] J.B. Wagner, Oxid. Met. 23 (1985) 251.
[72] B. Gillot, D. Garnier, Ann. Chim. Fr. 5 (1989) 483.
[73] J. Gillewicz-Wolter, K. Kowalska, Oxid. Met. 22 (1984) 101.
[74] J. Stringer, D.P. Whittle, Rev. Int. Ht. Temp. Refract. 14 (1977) 6.
[75] J. Stringer, in: I. Kirman, J.B. Marriott, M. Merz, P.R. Sahm, D.P. Whittle (Eds.), Proceedings of the International Conference on Behaviour of High Temperature Alloys in Aggressive Environments, Metals Society, London, 1980, p. 739.
[76] I. Wolf, H.J. Grabke, Solid State Commun. 54 (1985) 5.
[77] S. Mrowec, in: Proceedings of the 8th International Conference on Metallic Corrosion, vol. 3, Dechema, Frankfurt, 1981, p. 2110.
[78] K. Nishida, T. Narita, T. Tassi, S. Sesaki, Oxid. Met. 14 (1980) 65.
[79] E.A. Gulbransen, K.F. Andrew, J. Electrochem. Soc. 101 (1954) 128.
[80] S. Mrowec, K. Przybylski, High Temp. Mater. Process. 6 (1984) 1.
[81] D. Caplan, G.I. Sproule, Oxid. Met. 9 (1975) 459.
[82] O. Kubaschewski, C.B. Alcock, P.J. Spencer, Materials Thermochemistry, sixth ed., Pergamon, Oxford, 1993.
[83] T. Rosenquist, J.I.S.I. 176 (1954) 36.
[84] D.R. Holmes, R.B. Hill, L.M. Wyatt (Eds.), Corrosion of Steels in CO_2, Proceedings of the British Nuclear Energy Society International Conference at Reading University, British Nuclear Energy Society, London, 1974.
[85] G.B. Gibbs, Oxid. Met. 7 (1973) 173.